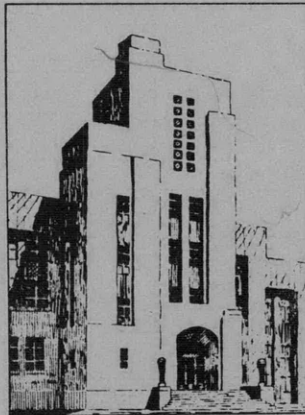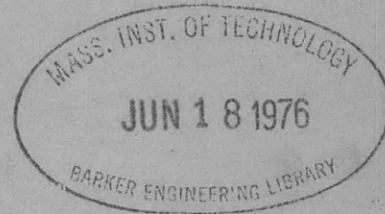#1

NAVY DEPARTMENT
THE DAVID W. TAYLOR MODEL BASIN
WASHINGTON 7, D.C.

THE CALCULATION OF THE VISCOUS DRAG
OF BODIES OF REVOLUTION

by

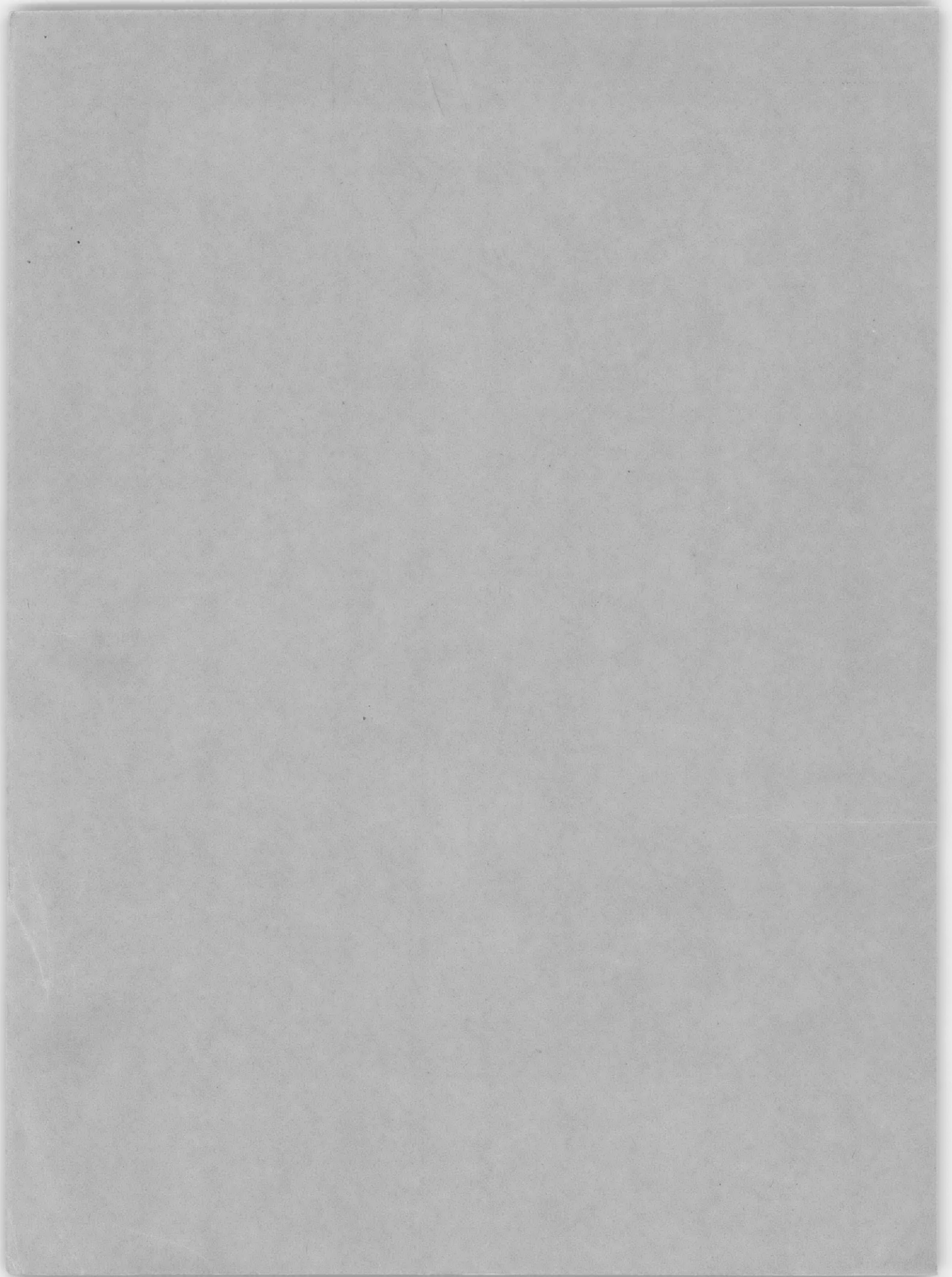Paul S. Granville

July 1953

Report 849

NS 715-102

THE CALCULATION OF THE VISCOUS DRAG OF
BODIES OF REVOLUTION

by

Paul S. Granville

TABLE OF CONTENTS

NOTATION

A	Area
a^*	Axisymmetric displacement thickness, Equation [12]
C	Constant in Mangler's transformations, Equation [42]
C_D	Drag coefficient, $D/\frac{1}{2}\rho\, U_\infty^2$
D	Total drag
D_f	Skin-friction drag
D_p	Pressure drag
e	Subscript for quantities at tail of body
g	Subscript for quantities at point where $\delta \ll r_w$ no longer holds
H	Two-dimensional shape parameter, δ^*/θ
h	Axisymmetric shape parameter, Λ^*/Ω
j	Exponent in Equation [76], $(1 + m)\,(H + 2)$
L	Length of body
l	Axial distance along body of revolution
m	Exponent of power law for local coefficient of skin friction, Equation [74]
N	Subscript for quantities at neutral stability point
n	Exponent of power law for velocity profiles, Equation [85]
p	Pressure in boundary layer
p_∞	Pressure of undisturbed incoming stream
q	Exponent in Equation [92]
q_ϕ	Velocity of fluid in ϕ-direction
q_ϕ'	Turbulent fluctuation in q_ϕ
R_L	Body Reynolds number, $L\,U_\infty/\nu$
R_θ	Boundary-layer Reynolds number, $\theta\,U/\nu$
r	Transverse radius from axis of body
r_w	Transverse radius to surface of body of revolution
r^*	Radius to equivalent body with added displacement thickness
t	Subscript for quantities at transition
tb	Subscript for quantities at transition point induced by free-stream turbulence

ts	Subscript for quantities at self-excited transition point
U	Velocity at outer edge of boundary layer
U_∞	Velocity of undisturbed incoming stream
u	Velocity of fluid parallel to surface of body in x-direction (mean velocity for turbulent flows)
u'	Turbulent fluctuation in u
v	Velocity of fluid normal to surface of body (mean velocity for turbulent flows)
v'	Turbulent fluctuation in v
x	Arc length along meridian profile
y	Distance normal to body surface
α	Angle between tangent to surface and axis of body
δ	Thickness of boundary layer
δ^*	Two-dimensional displacement thickness
ζ_0	Constant in power law for local coefficient of skin friction in Equation [74]
θ	Two-dimensional momentum thickness, $\displaystyle\int_0^\delta \left(1-\frac{u}{U}\right)\frac{u}{U}\,dy$
Λ^*	Displacement area, $\displaystyle\int_0^\delta \left(1-\frac{u}{U}\right) r\,dy$
μ	Viscosity of fluid
ν	Kinematic viscosity of fluid
ρ	Density of fluid
σ	Normal-stress term, $\rho\,\overline{u'^2}$
τ	Shearing stress, $\mu\dfrac{\partial u}{\partial y} - \rho\,\overline{u'v'}$
τ_w	Shearing stress at body surface
ϕ	Angle between a meridian plane and the reference meridian plane
Ω	Momentum area, $\displaystyle\int_0^\delta \left(1-\frac{u}{U}\right)\frac{u}{U} r\,dy$
Ω_∞	Momentum area of wake at infinity downstream
0	Subscript for quantities at zero pressure gradient on flat plates
$\sim$	Tilde over equivalent two-dimensional quantities

ABSTRACT

A procedure is presented for calculating the viscous drag of bodies of revolution in axial motion from boundary-layer theory. Rapid approximate methods are developed for computing the growth of the laminar and turbulent boundary layers. A new empirical criterion is given for locating the position of self-excited transition associated with low-turbulence flows.

INTRODUCTION

A completely immersed body moving rectilinearly with uniform velocity in an infinite fluid at rest experiences a resisting force which may be termed viscous drag as it results primarily from the viscous properties of the fluid. In designing low-drag bodies there often a-rises the need for calculating the viscous drag of streamlined bodies of revolution in axial motion when considering various proposed shapes. For bodies moving at high Reynolds numbers, which are of great technical importance, the viscous drag of streamlined bodies of revolution is readily amenable to analytical treatment on the basis of the boundary-layer concept.

Historically, the theoretical analysis of the drag of bodies in uniform motion by assuming an ideal (non-viscous) fluid gave the fruitless result of zero drag for all bodies, the classical D'Alembert paradox. At the other extreme, the theoretical analysis of drag by applying the complete set of Navier-Stokes equations of motion for the flow of a viscous fluid led, in general, to mathematical difficulties which were virtually unresolvable owing to the complicated non-linear nature of these equations. For bodies moving at high Reynolds numbers, however, the flow is virtually that of an ideal fluid except in a thin boundary layer next to the body where substantial viscous forces are produced by the rapid drop in velocity to zero at the body surface. Accordingly, by considering the viscous flow confined to the boundary layer, Prandtl was able to derive the simpler boundary-layer equations of motion from the Navier-Stokes equations.

The principal purpose of this report is to describe methods of solving the boundary-layer equations of motion to arrive at the viscous drag of bodies of revolution of arbitrary shape in uniform axial motion. The study is restricted to hydraulically or aerodynamically smooth streamlined bodies in incompressible flow. A streamlined body may be defined as one without appreciable separation of flow from its surface and consequently with small pressure drag resulting from the generation of separation eddies. It is to be noted, however, that some pressure drag is still present in the viscous drag of even perfectly streamlined shapes owing to the effect of the boundary layer in displacing the main flow outward, especially near the tail.

The calculation of the viscous drag of a body of revolution requires a detailed analysis of the development of each phase of the boundary layer from its origin on the nose of the body to its final phase as the frictional wake far downstream. In the downstream direction the

boundary layer may consist successively of: a laminar boundary layer, a transition zone from laminar to turbulent flow, a turbulent boundary layer, and a frictional wake.

In the laminar boundary layer an approximate method involving a simple quadrature is derived for the rapid calculation of the changes in momentum. The derivation consists of an extension to axisymmetric flows past bodies of revolution of a method of successive approximation introduced by Shvets[1] for two-dimensional laminar boundary layers.

New empirical criteria are presented for locating the position of transition for either low-turbulence or turbulent free-streams from the position of neutral stability. The position of so-called self-excited transition occurring in low-turbulence streams or under flight conditions is based on the average pressure gradient from the position of neutral stability to that of transition. Although the test data are for two-dimensional flows, the criterion is extended to axisymmetric flows past bodies of revolution by means of Mangler's transformations. An approximate criterion for estimating the position of transition on a body in a turbulent free-stream is established on the basis of measured positions of transition for flat plates in free streams with various degrees of turbulence.

The analysis of the axisymmetric turbulent boundary layer on a body of revolution is divided into that for the main portion of the body, where the boundary layer is relatively thin compared to the radius of the body, and that for the tail portion, where the boundary layer is relatively thick. The momentum changes in the thin boundary layer may be calculated by a rapid method involving a simple quadrature wherein a power-law relation for the skin friction of flat plates is incorporated. Flat-plate values for skin friction are deemed reliable even where the local skin friction is diminishing in an adverse pressure gradient owing to the compensating effect of the Reynolds normal-stress term. The turbulent boundary layer on the tail is analyzed by means of appropriate linear simplifications which give a rapid method for calculating the momentum changes. An expression is derived for the change in momentum produced by the pressure difference in the wake at the tail and in the wake far downstream in accordance with a method presented by Young[2] wherein, however, a more general relationship is employed for the variation of the shape parameter of the velocity profile.

For quick reference the various steps involved in calculating the development of the boundary layer on a body of revolution are summarized at the end of this report.

GENERAL CONSIDERATIONS

AXISYMMETRIC BOUNDARY-LAYER FLOW

The main elements comprising axisymmetric flow past a body of revolution at high Reynolds numbers are shown in Figure 1 for the meridian plane. Two principal regions of flow are indicated: the boundary layer next to the body with viscous flow and the region

---

[1]References are listed on page 29.

external to the boundary layer with essentially potential (non-viscous) flow. The pressure distribution along the body is mainly determined by the potential flow with only a slight modification arising from the boundary-layer flow except right at the tail where the after stagnation pressure of potential flows is absent. The pressure distribution on the body is important in determining the boundary-layer flow inasmuch as it is one of the most important factors governing the growth and development of the boundary layer. A negative pressure gradient is termed favorable and a positive pressure gradient adverse in connection with preventing separation of the boundary-layer flow from the body surface.

Starting as laminar flow at the stagnation point on the nose, the boundary-layer flow develops instability and undergoes transition to turbulent flow at some position downstream on the body. The boundary-layer flow usually continues turbulent for the remaining after portion of the body and leaves the tail as the frictional wake which extends indefinitely downstream.

VISCOUS DRAG

The viscous drag of a body is generally derivable from the boundary-layer flow either on the basis of the local forces acting on the surface of the body or on the basis of the velocity profile of the wake far downstream. The local hydrodynamic force on a unit of surface area is resolvable into a surface shearing stress or local skin friction τ_w tangent to the body surface and a pressure p normal to the surface. The summation over the whole body surface of the axial components of the local skin friction and of the pressure gives, respectively, the skin-friction drag D_f and the pressure drag D_p which for a body of revolution in axisymmetric flow become

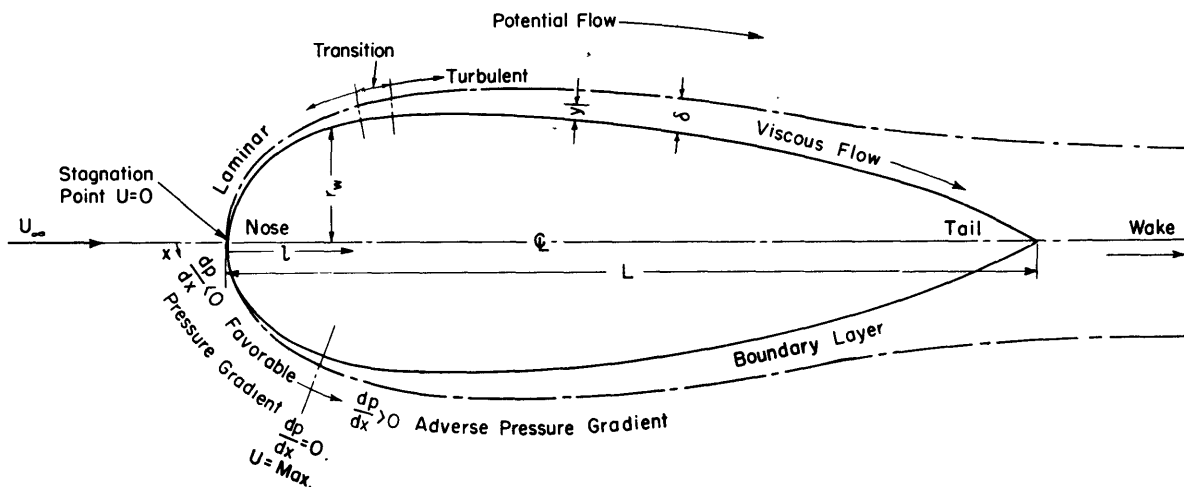$$D_f = 2\pi \int_0^{x_e} r_w \, \tau_w \, \cos \alpha \, dx \qquad [1]$$

Figure 1 - Typical Boundary Layer Around a Body of Revolution in a Meridian Plane

and

$$D_p = 2\pi \int_0^{x_e} r_w\, p \sin \alpha\, dx \qquad [2]$$

where r_w is the radius from the axis to the body surface,

α is the angle between the tangent to the meridian profile and the axis of the body,

x is the arc length along the meridian profile, and

x_e is the total arc length of the body from nose to tail.

The sum of the two drags then constitutes the total viscous drag D or

$$D = D_f + D_p \qquad [3]$$

The alternate procedure involving the velocity profile of the wake, which is better suited to the methods of this report, is to determine the total drag, without need of resolution into skin-friction and pressure drag, by considering the net rate of loss of momentum of the flow of the entire stream. The analytical procedure is to apply the momentum theorem of hydrodynamics to a control surface enclosing a region about the body with dimensions sufficiently large to have substantially undisturbed free-stream pressure p_∞ at its periphery. The total drag of the body which is the net rate of loss of momentum in the axial direction is then given by

$$D = 2\pi\rho \int_0^\infty u\left(U_\infty - u\right) r\, dr \qquad [4]$$

where U_∞ is the velocity of the incoming undisturbed stream ahead of the body,

u is the velocity in the wake far downstream,

r is the radial distance from the axis, and

ρ is the mass density of the fluid.

In terms of the momentum area of the wake far downstream

$$\Omega_\infty \equiv \int_0^\infty \frac{u}{U_\infty}\left(1 - \frac{u}{U_\infty}\right) r\, dr \qquad [5]$$

the drag is

$$D = 2\pi\rho\, U_\infty^2\, \Omega_\infty \qquad [6]$$

The drag coefficient C_D based on some appropriate reference area A is

$$C_D = \frac{D}{\frac{1}{2}\rho U_\infty^2\, A} = \frac{4\pi\Omega_\infty}{A} \qquad [7]$$

Inasmuch as the momentum area of the wake Ω_∞ is the final stage of the development of the boundary-layer flow from its inception on the nose of the body, it is necessary to cal-

culate the momentum area of the boundary-layer flow for each of its stages in order to determine the resulting drag of the body.

PRESSURE DISTRIBUTION ALONG THE BODY

Before any boundary-layer calculations can be performed for the body of revolution whose drag is to be determined, it is necessary to have on hand the distribution of pressure p along the body, which in non-dimensional terms is usually presented as

$$\frac{p - p_\infty}{\frac{1}{2}\rho U_\infty^2} = 1 - \left(\frac{U}{U_\infty}\right)^2 \tag{8}$$

Here p_∞ is the pressure of the undisturbed stream far ahead, and U is the velocity at the outer edge of the boundary layer.

Where no experimental values of pressure distribution are available, recourse can be had to methods for calculating the potential flow past the body which involve the solution of the Laplace equation for arbitrary boundary conditions. Such methods, which are reviewed briefly and evaluated in Reference 3, are, in general, numerically arduous and difficult to apply to bodies of arbitrary shape. Recently, Landweber[3] developed an accurate method, well suited to automatic calculating machines, in which a special iteration formula is employed in solving the resulting Fredholm integral equation of the first kind. A faster method, giving, however, only approximate results, is that of Young and Owen[4] which involves interpolation among tabulated values of Legendre polynomials.

For the original profile of the body of revolution the calculated pressure distribution for potential flow agrees closely with measured values over most of the length of the body, the greatest discrepancy appearing near the tail because of the displacement effect of the boundary layer. A closer result can be obtained, however, by repeating the potential-flow calculation for a somewhat altered body consisting of the original contour and an added thickness based on the displacement effect of the boundary layer. The added displacement thickness in the y-direction normal to the surface for a body of revolution in axisymmetric flow, as shown in Figure 2, is obtained by equating the total flow retarded in the boundary layer of thickness δ to the amount subtracted from the potential flow of thickness a^* or

$$\int_0^{a^*} 2\pi (U - 0)\, r\, dy = \int_0^{\delta} 2\pi (U - u)\, r\, dy \tag{9}$$

or

$$\int_0^{a^*} r\, dy = \int_0^{\delta} \left(1 - \frac{u}{U}\right) r\, dy \equiv \Lambda^* \tag{10}$$
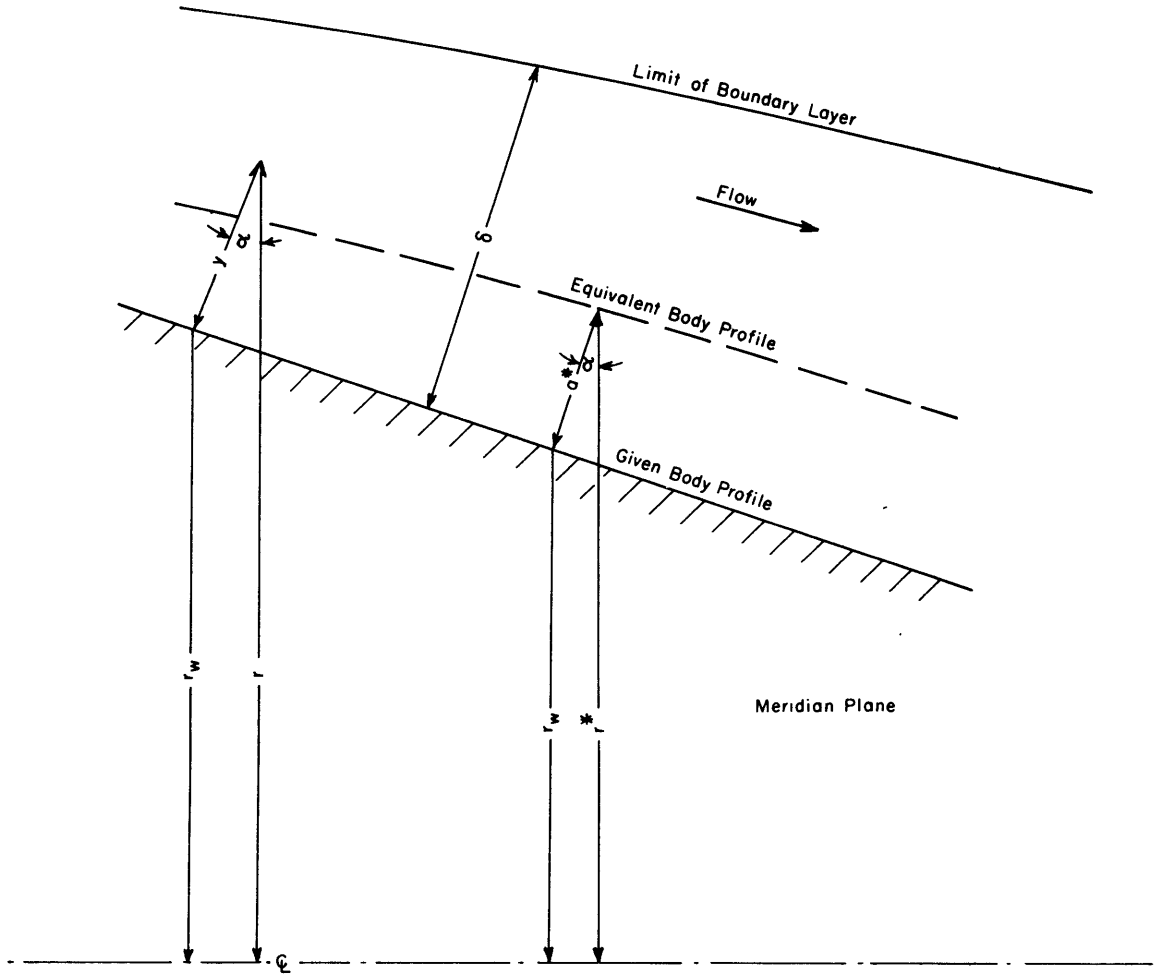
Figure 2 - Equivalent Body of Revolution with Displacement Thickness

where Λ^* is the displacement area. Substituting

$$r = r_w + y \cos \alpha \qquad [11]$$

in Equation [10] gives

$$a^* = \frac{-r_w + \sqrt{r_w^2 + 2\Lambda^* \cos \alpha}}{\cos \alpha} \qquad [12]$$

Over the forward part of the body where $\delta \ll r_w$, a^* reduces to

$$a^* = \int_0^\delta \left(1 - \frac{u}{U}\right) dy = \delta^* \qquad [13]$$

which is the displacement thickness for two-dimensional flow. In the wake where $r_w = 0$, Equation [12] reduces to

$$a^* = \sqrt{2\Lambda^*} \qquad [14]$$

It is convenient to define a radius r^* to the surface of the equivalent body, shown in Figure 2,

$$r^* = r_w + a^* \cos \alpha \qquad [15]$$

Then from [12]

$$r^* = \sqrt{r_w^2 + 2 \Lambda^* \cos \alpha} \qquad [16]$$

AXISYMMETRIC LAMINAR BOUNDARY LAYER

The solution of laminar boundary layers in either two-dimensional or axisymmetric flows has been the subject of numerous mathematical investigations owing to the interesting characteristics of the resulting equations of motion. The considerable literature that has developed contains methods of various degrees of complexity and precision which are given in the summaries by Goldstein[5] and more recently in the AVA Monographs[6] and by Schlichting.[7] For many drag calculations very precise solutions of the boundary layer, requiring extensive numerical work, are usually not warranted, especially where the laminar boundary layer constitutes a small part of the whole boundary layer. A simple approximate formula, well adapted to drag calculations, will be devised by an extension to axisymmetric flow of a method of successive approximation introduced by Shvets[1] for two-dimensional flows.

Owing to the thinness of the laminar boundary layer on the forward part of the body, $\delta \ll r_w$, the equations of motion for steady axisymmetric boundary-layer flow past a body of revolution with negligible longitudinal curvature (Reference 5) reduce to

$$u \frac{\partial u}{\partial x} + v \frac{\partial u}{\partial y} = - \frac{1}{\rho} \frac{\partial p}{\partial x} + \nu \frac{\partial^2 u}{\partial y^2}$$

$$0 = \frac{\partial p}{\partial y} \qquad [17]$$

and the equation of continuity reduces to

$$\frac{\partial u}{\partial x} + \frac{\partial v}{\partial y} + \frac{u}{r_w} \frac{dr_w}{dx} = 0 \qquad [18]$$

Here u and v are the x- and y-components of the boundary-layer velocity respectively parallel and normal to the surface of the body in the meridian plane, p is the pressure in the boundary layer, ν is the kinematic viscosity of the fluid, and δ is the thickness of the boundary layer in the y-direction. These equations have been shown[8] to remain applicable at the forward stagnation point for bodies with blunt noses even though both δ, $r_w \to 0$. The following boundary conditions are to be satisfied by the boundary-layer equations:

$$u = 0 \quad \text{at} \quad y = 0$$
$$u = U \quad \text{at} \quad y = \delta \qquad [19]$$

The pressure p and the velocity U at the outer edge of the boundary layer are related by Bernouilli's equation for potential flow

$$p + \frac{1}{2} \rho U^2 = \text{constant} \qquad [20]$$

or

$$-\frac{1}{\rho} \frac{dp}{dx} = U \frac{dU}{dx} \qquad [21]$$

Combining the equation of motion, [17], the continuity equation, [18], and the differential Bernouilli equation, [21], produces

$$\nu \frac{\partial^2 u}{\partial y^2} = u \frac{\partial u}{\partial x} - \frac{\partial u}{\partial y} \int_0^y \left(\frac{\partial u}{\partial x} + \frac{u}{r_w} \frac{dr_w}{dx} \right) dy - U \frac{dU}{dx} \qquad [22]$$

A first approximation is to let

$$\nu \frac{\partial^2 u}{\partial y^2} = 0 \qquad [23]$$

Integrating [23] twice and utilizing boundary conditions, [19], results in a linear velocity profile

$$\frac{u}{U} = \frac{y}{\delta} \qquad [24]$$

A second approximation is obtained by substituting the linear velocity profile, [24], into differential equation [22]. Integrating twice and utilizing boundary conditions, [19], as before gives

$$\nu \frac{u}{U} = \frac{\delta^2}{24} \frac{dU}{dx} \left[\left(\frac{y}{\delta} \right)^4 - 12 \left(\frac{y}{\delta} \right)^2 + 11 \left(\frac{y}{\delta} \right) \right]$$

$$-\frac{\delta}{24} U \left(\frac{d\delta}{dx} + \frac{\delta}{r_w} \frac{dr_w}{dx} \right) \left[\left(\frac{y}{\delta} \right)^4 - \left(\frac{y}{\delta} \right) \right] + \nu \frac{y}{\delta} \qquad [25]$$

Applying the additional boundary condition that

$$\frac{\partial u}{\partial y} = 0 \quad \text{at} \quad y = \delta \qquad [26]$$

to the differentiated form of Equation [25] yields

$$\frac{d(r_w \delta)^2}{dx} + \frac{6}{U} \frac{dU}{dx} (r_w \delta)^2 = \frac{16 \nu r_w^2}{U} \qquad [27]$$

For a linear velocity profile, [24],

$$\theta = \frac{\delta}{6} \tag{28}$$

where θ is the two-dimensional momentum thickness

$$\theta \equiv \int_0^\delta \frac{u}{U}\left(1 - \frac{u}{U}\right)dy \tag{29}$$

Substituting θ in [27] gives

$$\frac{d(r_w\,\theta)^2}{dx} + \frac{6}{U}\frac{dU}{dx}(r_w\,\theta)^2 = \frac{4}{9}\frac{\nu r_w^{\;2}}{U} \tag{30}$$

Integrating the linear differential equation, [30], produces

$$(r_w\,\theta)^2 = \frac{4}{9}\frac{\nu}{U^6}\int_0^x r_w^{\;2}\;U^5\;dx \tag{31}$$

with the stagnation point $x = 0$ as the initial point of integration. An interesting feature of this result is its being identical in both form and numerical constants to the semi-empirical result of Thwaites[9] when his two-dimensional solution is extended to the axisymmetric case.[10] Thwaites averaged known solutions of two-dimensional laminar boundary layers for a variety of pressure gradients.

Now the momentum area Ω for axisymmetric boundary-layer flow in general may be defined as

$$\Omega \equiv \int_0^\delta \frac{u}{U}\left(1 - \frac{u}{U}\right)r\,dy \tag{32}$$

Since

$$r = r_w + y\cos\alpha \tag{11}$$

with

$$0 \leq y \leq \delta$$
$$0 \leq \cos\alpha \leq 1 \tag{33}$$

then in general

$$r_w\,\theta < \Omega < (r_w + \delta)\,\theta \tag{34}$$

Hence for $\delta \ll r_w$ which is the case under consideration

$$\Omega = r_w\,\theta \tag{35}$$

A non-dimensional form of the momentum equation, [31], convenient for calculation purposes is

$$\left(\frac{\Omega}{L^2}\right)^2 = \left(\frac{r_w\,\theta}{L^2}\right)^2 = \frac{4}{9}\,\frac{1}{R_L\left(\dfrac{U}{U_\infty}\right)^6}\int_0^{l/L}\left(\frac{r_w}{L}\right)^2\left(\frac{U}{U_\infty}\right)^5\sec\alpha\;d\!\left(\frac{l}{L}\right)\qquad [36]$$

where l is the axial distance from the nose,

$$dl = \cos\alpha\,dx \qquad [37]$$

L is the length of the body and R_L is the body Reynolds number given by

$$R_L = \frac{U_\infty L}{\nu} \qquad [38]$$

Transition to turbulent flow is assumed to occur instantaneously at a transition point $(l/L)_t$ which then becomes the upper limit of integration in Equation [36] when the integration is performed for the complete laminar boundary layer.

TRANSITION

As the boundary layer thickens downstream on the body, the laminar flow tends to become unstable and undergo transition to turbulent flow under the stimulus of disturbances in the flow. The transition zone may be considered to extend from the point where the characteristic shape of the mean-velocity profile of the laminar boundary layer begins to change to the point where the characteristic shape of the mean-velocity profile of the turbulent boundary layer first appears. For most drag calculations the zone of transition is short enough to be adequately represented by a transition point. The position of transition depends largely upon the interaction of the boundary-layer flow with random disturbances in the flow. Significant parameters of the boundary-layer flow affecting the position of transition are the boundary-layer Reynolds number representing the ratio of inertial forces to viscous forces, the pressure gradient in the downstream direction, and the curvature of the surface. The source of random disturbances may be the turbulence in the free stream, the roughness of the surface or noise being transmitted through the fluid.

As shown theoretically by Tollmien[11] and Schlichting[7] among others (see summary in Reference 12) and verified experimentally by Schubauer and Skramstad[13] and Liepmann,[14] the laminar boundary layer exhibits stability characteristics which are governed largely by the boundary-layer Reynolds number and by the pressure gradient. Random disturbances of vanishingly small amplitude have certain frequencies amplified and other frequencies damped by the laminar flow in the boundary layer. The amplified fluctuations combine into regular waves termed Tollmien-Schlichting waves which increase in amplitude downstream at a rate determined by the Reynolds number and the pressure gradient of the boundary layer. Intermittent

bursts of high-frequency fluctuations which are associated with intermittent separations of the laminar flow herald the arrival of the more random fluctuations characteristic of fully developed turbulent flow. The transition just described, which depends on the amplification of vanishingly small disturbances, may be termed self-excited transition.

Disturbances of greater amplitude arising from free-stream turbulence or rough surfaces tend to hasten the decomposition of the laminar boundary layer into a turbulent boundary layer. Taylor[15] has developed the concept of momentary separations arising from momentary adverse pressure gradients as the mechanism instigating turbulent motion. In accordance with Taylor's analysis both the scale and intensity of the free-stream turbulence have been shown experimentally[16] to have a marked bearing on the position of transition.

The studies of Liepmann[14,17] on the stability of laminar boundary layers on curved surfaces have shown the Tollmien-Schlichting type of stability to exist on surfaces convex to the flow and the Görtler type of stability involving vortices to exist on concave surfaces. Convex surfaces have a greater stabilizing effect and concave surfaces a lesser stabilizing effect than flat surfaces.

The presence both of large boundary-layer Reynolds numbers and of adverse pressure gradients tends to promote transition by increasing the instability of the laminar boundary layer and by accelerating the amplification of the Tollmien-Schlichting waves.

Under special circumstances transition is hastened when the laminar boundary layer separates from the body and reattaches itself as a turbulent boundary layer. Such separation may be caused by sharp adverse pressure gradients[18] on bodies at large angles of attack or by sharp adverse pressure gradients induced by large single roughnesses obstructing the flow.[19]

Quantitative criteria for establishing the transition points on smooth bodies of revolution will be considered here for two technically important flow situations which are characterized by the absence or presence of significant amounts of turbulence in the main flow stream. Zero or low-turbulence condition exists in specially constructed low-turbulence wind tunnels while a condition of various degrees of turbulence is present in most wind tunnels and flow facilities. The flight of aircraft is considered a case of low turbulence on the basis of tests by Jones[20] who concluded that the scale of turbulence in the atmosphere is such as to have no effect on transition. A similar low-turbulence condition may be assumed in the case of bodies moving in the depths of the oceans where currents are absent.

Transition in the low-turbulence case may be considered to be of the Tollmien-Schlichting type wherein vanishingly small disturbances are amplified in the boundary layer to the castastrophic point of resulting turbulence within the boundary layer. The stability analysis of laminar boundary layers shows the existence of a point of neutral stability wherein the immediate neighborhood upstream disturbances of all frequencies are damped out. Mangler[21] has prepared a chart, partly reproduced in Figure 3, which specifies the neutral stability point in terms of the critical value $R_{\theta,N}$ of boundary-layer Reynolds number R_θ where
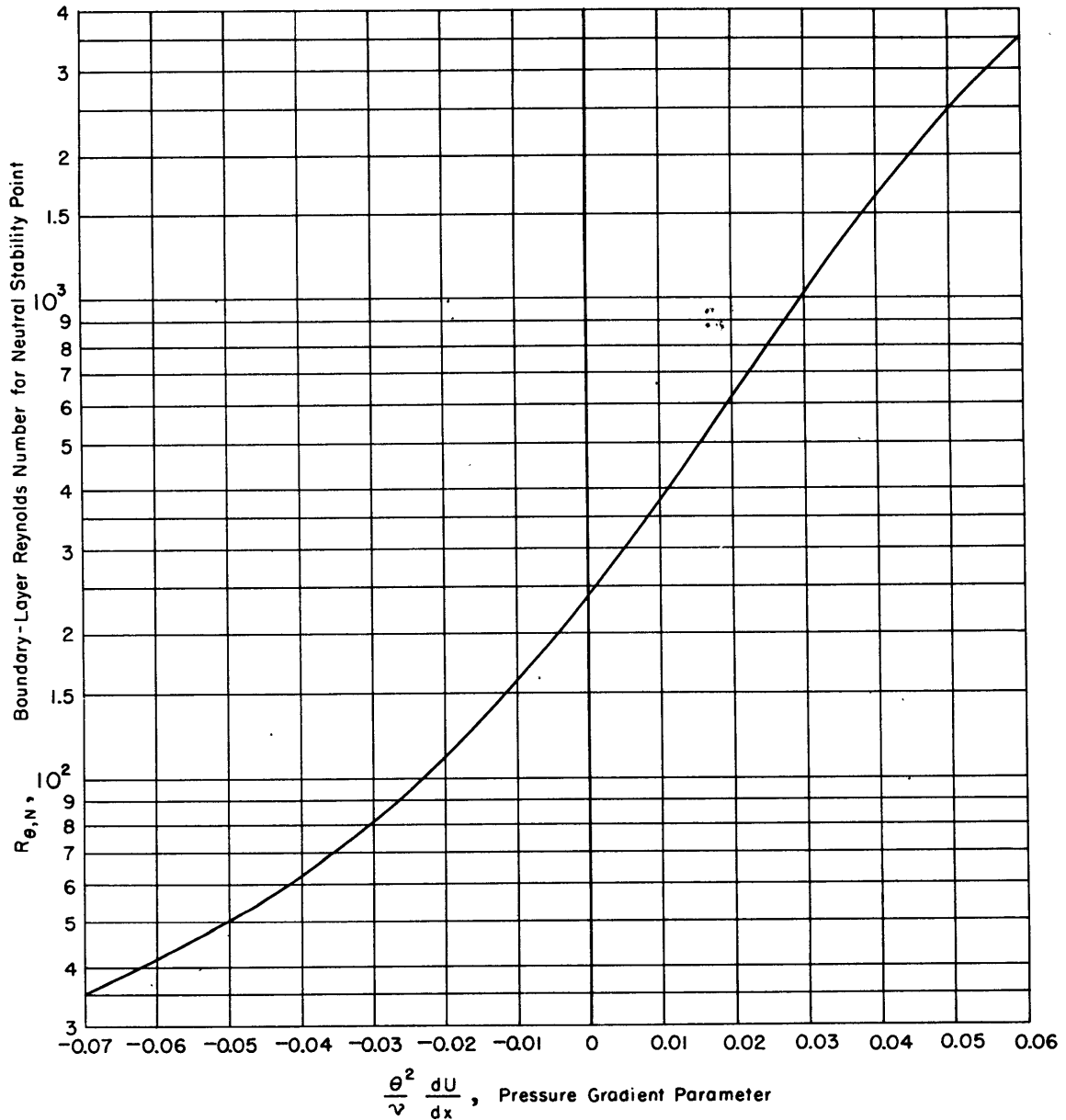
Figure 3 - Neutral Stability Point as Function of Pressure Gradient (Mangler, Ref. 21)

$$R_\theta = \frac{\theta U}{\nu} \qquad [39]$$

as a function of a pressure-gradient parameter $\frac{\theta^2}{\nu}\frac{dU}{dx}$. The curve shown, which is based on the stability characteristics of Pohlhausen-type velocity profiles as calculated by Schlichting and Ulrich[22] is applicable to both two-dimensional and axisymmetric boundary layers.

Unfortunately no theoretical analysis has been developed for locating the point of self-excited transition from the amplification of the Tollmien-Schlichting waves past the point of neutral stability. Experimental evidence[13] indicates a pronounced effect by favorable pressure

gradients in damping and adverse pressure gradients in amplifying the Tollmien-Schlichting waves.

A rough empirical criterion for locating the point of self-excited transitions is ascribed to Walz[23] who suggests a critical value of the Reynolds number of transition $R_{\theta,ts}$ as thrice that for neutral stability or

$$R_{\theta,ts} = 3 R_{\theta,N} \tag{40}$$

There follows, however, a new empirical criterion which is based on more rational grounds and which attempts to incorporate the effect of pressure gradients in determining the position of self-excited transition. Since the transition point depends on the cumulative effect of the pressure gradients from neutral stability to transition, it would seem appropriate to use as a first approximation the average pressure gradient for one of the significant parameters. Accordingly two-dimensional data on transition points from tests on wing sections in flight[20,24] and in low-turbulence wind tunnels[13,25,26] were analyzed on this basis. As shown in Figure 4 the difference in Reynolds numbers from the point of neutral stability to transition

$\widetilde{R}_{\theta,ts} - \widetilde{R}_{\theta,N}$ is plotted against the average pressure gradient parameter $\overline{\dfrac{\widetilde{\theta}^2}{\nu}\dfrac{d\widetilde{U}}{d\widetilde{x}}}$ over the same region where

$$\overline{\frac{\widetilde{\theta}^2}{\nu}\frac{d\widetilde{U}}{d\widetilde{x}}} \equiv \frac{\displaystyle\int_{\widetilde{x}_N}^{\widetilde{x}_{ts}} \frac{\widetilde{\theta}^2}{\nu}\frac{d\widetilde{U}}{d\widetilde{x}}\,d\widetilde{x}}{\displaystyle\int_{\widetilde{x}_N}^{\widetilde{x}_{ts}} d\widetilde{x}} \tag{41}$$

The tildes over the symbols refer to two-dimensional flows. Examination of the plotted data in Figure 4 indicates a reasonably consistent variation between the two parameters involved.

The conversion of the preceeding two-dimensional data for use in axisymmetric flows past bodies of revolution may be accomplished by means of Mangler's relations[7,21] for transforming the equation of motion of two-dimensional boundary layers to those of equivalent axisymmetric boundary layers on bodies of revolution. Mangler's transformation relations are

$$d\widetilde{x} = C^2 \frac{r_w^2}{L^2}\, dx$$

$$\widetilde{y} = C\,\frac{r_w}{L}\, y \tag{42}$$

$$\widetilde{\theta} = C\,\frac{r_w}{L}\, \theta$$

$$\widetilde{U}(\widetilde{x}) = U(x)$$

Difference Between Reynolds Numbers of Neutral Stability and Transition

$\left(\widetilde{R}_{\theta,ts} - \widetilde{R}_{\theta,N}\right)$,

2000

1800

1600

1400

1200

1000

800

600

400

200

0

-0.04   -0.03   -0.02   -0.01   0   0.01   0.02   0.03   0.04

$\dfrac{\widetilde{\theta}^2}{\nu} \dfrac{d\,\widetilde{U}}{d\,\widetilde{x}}$, Average Pressure Gradient from Neutral Stability Point to Transition Point

Low-Turbulence Wind Tunnel
● Suction Side ⎫ Braslow and Visconti, Ref.(26),
+ Pressure Side ⎰   NACA Airfoil $65_{(215)}-114$
X Von Doenhoff, Ref.(25), NACA Airfoil 0012
O Schubauer and Skramstad, Ref.(13), Flat Plate

Flight
□ Jones, Ref.(20), Wing Section 18 percent Thick
Δ Zalovcik and Skoog,(24), Low-Drag
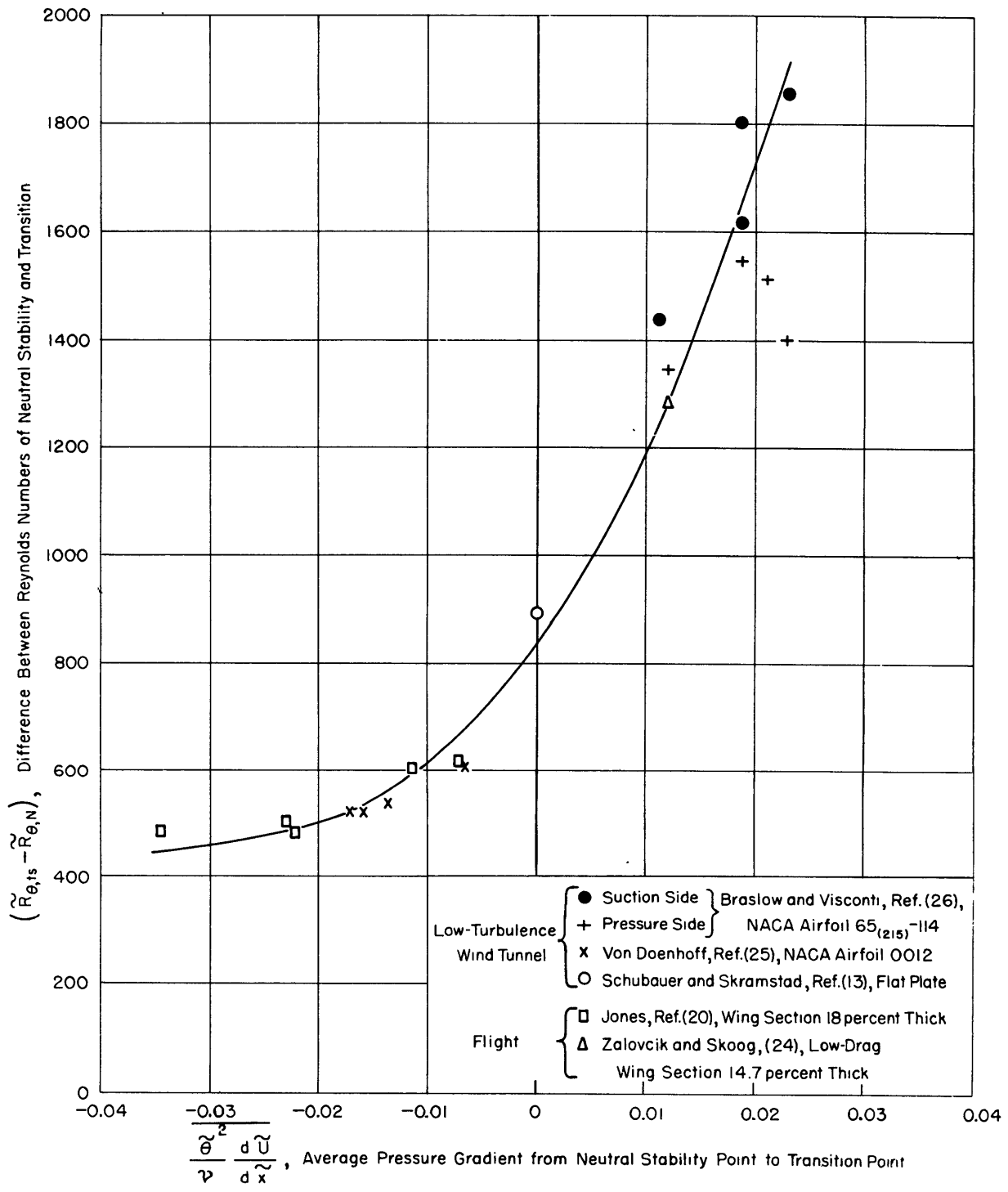Wing Section 14.7 percent Thick

Figure 4 - Position of Self-Excited Transition as Function of Average Pressure Gradient

where the tildes over the quantities refer to equivalent two-dimensional conditions and C is an arbitrary constant.

A simple expression will now be derived for $\overline{\dfrac{\tilde{\theta}^2}{\nu}\dfrac{d\tilde{U}}{d\tilde{x}}}$ which can be used to analyze two-dimensional data and which can be extended into an equivalent axisymmetric system. First the following two-dimensional momentum equation is obtained from the axisymmetric momentum equation, [30], by utilizing Mangler's relations [42]

$$\frac{d\tilde{\theta}^2}{d\tilde{x}} + \frac{6}{\tilde{U}}\frac{d\tilde{U}}{d\tilde{x}}\tilde{\theta}^2 = \frac{4}{9}\frac{\nu}{\tilde{U}} \tag{43}$$

Since in general

$$\frac{\tilde{\theta}^2}{\nu}\frac{d\tilde{U}}{d\tilde{x}} = \frac{1}{\nu}\frac{d(\tilde{U}\tilde{\theta}^2)}{d\tilde{x}} - \frac{\tilde{U}}{\nu}\frac{d\tilde{\theta}^2}{d\tilde{x}} \tag{44}$$

then from [43]

$$\frac{\tilde{\theta}^2}{\nu}\frac{d\tilde{U}}{d\tilde{x}} = \frac{4}{45} - \frac{1}{5\nu}\frac{d(\tilde{U}\tilde{\theta}^2)}{d\tilde{x}} \tag{45}$$

Averaging $\dfrac{\tilde{\theta}^2}{\nu}\dfrac{d\tilde{U}}{d\tilde{x}}$ over the distance from neutral stability to transition in accordance with [41] gives simply

$$\overline{\frac{\tilde{\theta}^2}{\nu}\frac{d\tilde{U}}{d\tilde{x}}} = \frac{4}{45} - \frac{1}{5\nu}\left[\frac{(\tilde{U}\tilde{\theta}^2)_{ts} - (\tilde{U}\tilde{\theta}^2)_N}{\tilde{x}_{ts} - \tilde{x}_N}\right] \tag{46}$$

In order to use the two-dimensional data of Figure 4 to determine the self-excited transition point for axisymmetric flow, it is necessary to express $\overline{\dfrac{\tilde{\theta}^2}{\nu}\dfrac{d\tilde{U}}{d\tilde{x}}}$ in terms of an equivalent axisymmetric system. Applying Mangler's transformations to [45] and integrating in accordance with [41] gives $\overline{\dfrac{\tilde{\theta}^2}{\nu}\dfrac{d\tilde{U}}{d\tilde{x}}}$ in equivalent axisymmetric quantities as

$$\overline{\frac{\tilde{\theta}^2}{\nu}\frac{d\tilde{U}}{d\tilde{x}}} = \frac{4}{45} - \frac{1}{5\nu}\left[\frac{\left(\frac{r_w^2}{L^2}U\theta^2\right)_{ts} - \left(\frac{r_w^2}{L^2}U\theta^2\right)_N}{\int_{x_N}^{x_{ts}}\frac{r_w^2}{L^2}dx}\right] \tag{47}$$

Furthermore, in order to use the two-dimensional data of Figure 4 to determine the self-excited transition points for axisymmetric flows, it is necessary to convert the Reynolds number for self-excited transition in two-dimensional flows $\tilde{R}_{\theta,ts}$ to that for axisymmetric flows on bodies of revolution $R_{\theta,ts}$. Now Mangler's transformations [42] give for all Reynolds numbers of laminar flows

$$\tilde{R}_\theta = C \, \frac{r_w}{L} \, R_\theta \qquad\qquad [48]$$

Owing to the presence of the arbitrary constant C, it is obvious that Mangler's transformations are not sufficient to determine the critical values of the Reynolds numbers for transition. Hence, other considerations must apply. In the analysis of the stability of laminar flows on bodies of revolution, it was found[6,21] that the resulting linearized equation of the disturbed flow at the limiting condition of large Reynolds numbers was the same as that for two-dimensional flows. Hence

$$\tilde{R}_{\theta, N} = R_{\theta, N} \qquad\qquad [49]$$

and as stated previously, the neutral stability chart of Figure 3 is applicable to both two-dimensional and axisymmetric flows on bodies of revolution. As a first approximation a similar condition will be assumed to hold for self-excited transition. Then

$$\tilde{R}_{\theta, ts} \cong R_{\theta, ts} \qquad\qquad [50]$$

As a check on the essential validity of the preceding, the self-excited transition points were computed for Lyon's[27] bodies of revolution on the basis of Figure 4. Owing to the non-existence of low-turbulence wind tunnels at the time of Miss Lyon's tests, the condition of least degree of turbulence represented in her tests was that when the turbulence-producing screens were not inserted in the wind tunnel. Comparison is then made in Table 1 of the axial locations l/L of the computed neutral stability points and self-excited transition points with the test data for the no-screen condition.

TABLE 1

Axial Locations l/L of Transition Data for Lyon's Bodies of Revolution[27]

Subject	Model A $R_L = 2.09 \times 10^6$	Model B $R_L = 2.075 \times 10^6$
Computed Neutral Stability Point	0.20	0.13
Computed Self-Excited Transition Point	0.56	0.7
Measured Transition Region (without screen)	0.50 - 0.70	0.30 - 0.35
Regions of Favorable Pressure Gradient	0 - 0.30	0 - 0.13 0.40 - 0.61
Regions of Adverse Pressure Gradient	0.30 - 1	0.13 - 0.40 0.61 - 1

The measured transition points should be behind the neutral stability points and forward of the self-excited transition points owing to the small amount of natural turbulence in the wind tunnel. Examination of Table 1 confirms this. The reason for the large difference between the measured transition point and the self-excited transition point on Model B is due to the favorable pressure gradient, $0.40 < l/L < 0.61$, which tends to delay the development of self-excited transition.

In order to obtain the neutral stability and transition points, it is more convenient to use nondimensional relations. From [36] there results

$$\frac{R_\theta^2}{R_L} = \frac{4}{9} \frac{1}{\left(\frac{U}{U_\infty}\right)^4 \left(\frac{r_w}{L}\right)^2} \int_0^{l/L} \left(\frac{U}{U_\infty}\right)^5 \left(\frac{r_w}{L}\right)^2 \sec\alpha \ d\left(\frac{l}{L}\right) \qquad [51]$$

It also follows that

$$\frac{\theta^2}{\nu} \frac{dU}{dx} = \left(\frac{R_\theta^2}{R_L}\right) \frac{1}{\left(\frac{U}{U_\infty}\right)^2} \frac{d\left(\frac{U}{U_\infty}\right)}{d\left(\frac{l}{L}\right)} \cos\alpha \qquad [52]$$

Thus, from [47]

$$\frac{\widetilde{\theta^2}}{\nu} \frac{d\widetilde{U}}{d\widetilde{x}} = \frac{4}{45} - \frac{1}{5} \left\{ \frac{\left[\frac{\left(\frac{R_\theta^2}{R_L}\right)\left(\frac{r_w}{L}\right)^2}{\left(\frac{U}{U_\infty}\right)}\right]_{ts} - \left[\frac{R_\theta^2}{R_L} \frac{\left(\frac{r_w}{L}\right)^2}{\left(\frac{U}{U_\infty}\right)}\right]_N}{\int_{\left(\frac{l}{L}\right)_N}^{\left(\frac{l}{L}\right)_{ts}} \left(\frac{r_w}{L}\right)^2 \sec\alpha \ d\left(\frac{l}{L}\right)} \right\} \qquad [53]$$

The neutral stability point or self-excited transition point is determined graphically by the intersection of a curve representing the appropriate parameters of the given boundary layer with the curves of Figure 3 or 4, as the case may be.

The position of transition on a body in a wind tunnel or other flow facility depends, to a great extent, upon the scale and intensity of the turbulence in the free stream. To simplify the analysis the representative measure of turbulence in the stream will be taken as the ratio of the root mean square of the velocity fluctuations in the x-direction to the mean velocity of the free stream or $\sqrt{u'^2}/U_\infty$. Data for flat plates without pressure gradient from tests in wind tunnels [13,28,29] are plotted in Figure 5, the ordinates being the difference in the boundary-layer Reynolds numbers for transition and that for neutral stability $R_{\theta,tb} - R_{\theta,N}$ and the abscissae being the percentage of turbulence $\sqrt{u'^2}/U_\infty$ in the free stream. It is to be noted that for flat plates the neutral stability point seems to be the limiting position of transition for streams of increasing turbulence while the self-excited transition point is the limiting position of transition for streams of decreasing turbulence.
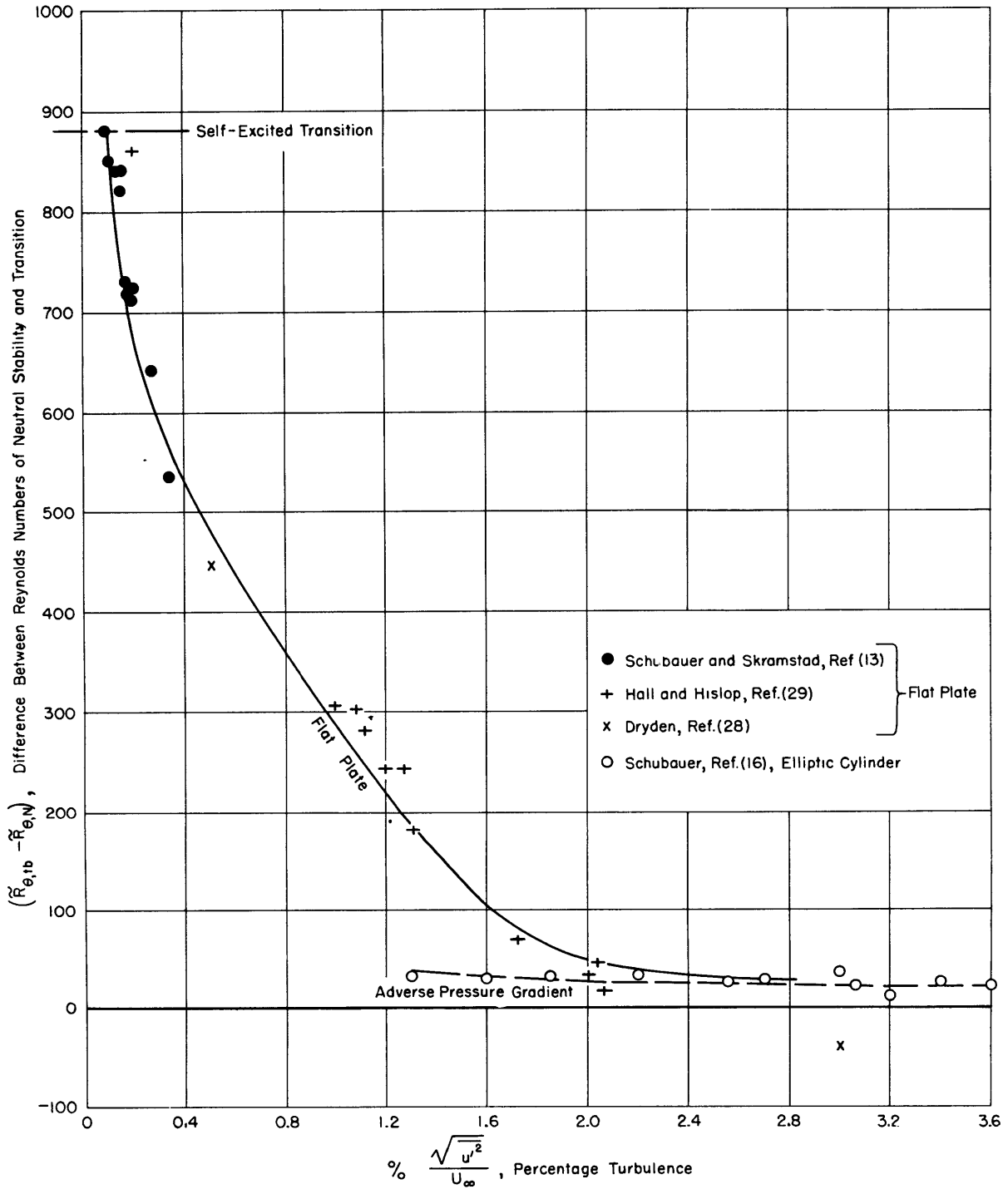
Figure 5 - Position of Transition in a Turbulent Stream

A similar trend for boundary layers with pressure gradients is indicated by the test data for the flow over an elliptic cylinder[16] as plotted in Figure 5. On the basis of the neutral stability point and the self-excited transition point as the lower and upper limiting positions of transition for boundary layers with pressure gradients in general, a rough criterion may be established for estimating the position of transition on bodies immersed in streams containing

turbulence. If the curve for transition for any boundary layer with a pressure gradient is assumed geometrically similar to that for a flat plate as plotted in Figure 5, the Reynolds number for transition $R_{\theta, tb}$ for boundary layers on bodies in a stream with turbulence may be stated as

$$\frac{R_{\theta, tb} - R_{\theta, N}}{R_{\theta, ts} - R_{\theta, N}} = \left(\frac{R_{\theta, tb} - R_{\theta, N}}{R_{\theta, ts} - R_{\theta, N}}\right)_0 \qquad [54]$$

where the subscript 0 refers to flat-plate values without pressure gradient. For more precise results, it is best to depend upon measured locations of the position of transition to obtain values of the Reynolds numbers for transition characteristic of the particular wind tunnel or flow facility being utilized.

AXISYMMETRIC TURBULENT BOUNDARY LAYER

GENERAL

Owing to the incomplete state of present knowledge, concerning the mechanics of turbulent flow processes, the analysis of turbulent boundary layers lacks the clearly defined features of laminar boundary layers. In order to arrive at results of immediate utility, extensive reliance has to be placed on empirical data to augment theoretically derived relations.

Turbulent flows, in general, may be treated from the Reynolds viewpoint, this considers turbulent flow to consist of a mean flow upon which a fluctuation flow of much smaller magnitude is superimposed. After the combined mean and fluctuation quantities are substituted into the Navier-Stokes equations of motion for viscous flow, appropriate time averages of the resulting flow lead to the Reynolds equations of motion containing separate terms for the mean quantities and the fluctuation quantities. The form of the Reynolds equations is similar to the Navier-Stokes equations with the significant exception of the presence of additional terms which consist of averages of various products of the fluctuation velocities. These additional terms may be shown to act as apparent stresses (Reynolds stresses) within the flow. It is, however, the present lack of analytical relations for the Reynolds stresses which has made the theoretical treatment of turbulent flows so difficult.

Turbulent boundary-layer equations are derived from the Reynolds equations in the same way as laminar boundary-layer equations are derived from the Navier-Stokes equations, i.e., by the process of eliminating terms of negligible magnitude.

In the case of axisymmetric flow past a body of revolution with negligible longitudinal curvature, the Reynolds equations of motion become*

---

*The Reynolds equations of motion for general curvilinear coordinates are written in tensor notation in Reference 30.

$$u \frac{\partial u}{\partial x} + v \frac{\partial u}{\partial y} + \frac{1}{\rho} \frac{\partial p}{\partial x} = \frac{\nu}{r} \frac{\partial}{\partial y} \left[r \left(\frac{\partial u}{\partial y} - \frac{\partial v}{\partial x} \right) \right] + \frac{1}{\rho r} \frac{\partial}{\partial x} \left[r \left(- \rho \overline{u'^2} \right) \right]$$

$$+ \frac{1}{\rho r} \frac{\partial}{\partial y} \left[r \left(- \rho \overline{u'v'} \right) \right] + \frac{\overline{q_\phi'^2}}{r} \frac{\partial r}{\partial x}$$

$$u \frac{\partial v}{\partial y} + u \frac{\partial v}{\partial y} + \frac{1}{\rho} \frac{\partial p}{\partial y} = \frac{\nu}{r} \frac{\partial}{\partial x} \left[r \left(\frac{\partial v}{\partial x} - \frac{\partial u}{\partial y} \right) \right] + \frac{1}{\rho r} \frac{\partial}{\partial y} \left[r \left(- \rho \overline{v'^2} \right) \right]$$

$$+ \frac{1}{\rho r} \frac{\partial}{\partial x} \left[r \left(- \rho \overline{u'v'} \right) \right] + \frac{\overline{q_\phi'^2}}{r} \frac{\partial r}{\partial y} \qquad [55]$$

$$0 = \frac{\partial}{\partial x} \left[r \left(- \rho \overline{u' q_\phi'} \right) \right] + \frac{\partial}{\partial y} \left[r \left(- \rho \overline{v' q_\phi'} \right) \right]$$

$$+ \left(- \rho \overline{u' q_\phi'} \right) \frac{\partial r}{\partial x} + \left(- \rho \overline{v' q_\phi'} \right) \frac{\partial r}{\partial y}$$

and the equations of continuity

$$\frac{\partial (ru)}{\partial x} + \frac{\partial (rv)}{\partial y} = 0 \qquad [56]$$

$$\frac{\partial (ru')}{\partial x} + \frac{\partial (rv')}{\partial y} = 0 \qquad [57]$$

The unprimed quantities refer to the mean flow and the primed quantities to the fluctuation flow. The bars over the various products indicate averages in accordance with the Reynolds concept. Specifically, u, v, q_ϕ, primed or unprimed, represent components of velocity in the x, y, and ϕ directions, respectively. As before, x is the distance along the meridian profile and y is the distance perpendicular to the profile. ϕ is the angle between any meridian plane and some reference meridian plane.

Eliminating terms of negligible magnitude in [55] gives the following equations of motion for the axisymmetric boundary layer on a body of revolution

$$u \frac{\partial u}{\partial x} + v \frac{\partial u}{\partial y} = - \frac{1}{\rho} \frac{\partial p}{\partial x} - \frac{1}{\rho r} \frac{\partial (r \sigma)}{\partial x} + \frac{1}{\rho r} \frac{\partial (r \tau)}{\partial y}$$

$$0 = \frac{\partial p}{\partial y} \qquad [58]$$

where

$$\sigma = \rho \overline{u'^2} \qquad [59]$$

is the negative value of a Reynolds normal stress and

$$\tau = \mu \frac{\partial u}{\partial y} - \rho \overline{u'v'} \qquad [60]$$

is the total shearing stress.

Integrating the boundary-layer equations, [58], across the boundary layer in the y-direction from $y = 0$ to $y = \delta$ and incorporating the equation of continuity, [56], gives the dif-

ferential form of the momentum equation for axisymmetric turbulent boundary layers on bodies of revolution

$$\frac{d\Omega}{dx} + (h + 2)\, \frac{\Omega}{U}\, \frac{dU}{dx} = r_w\, \frac{\tau_w}{\rho U^2} + \frac{1}{\rho U^2}\, \frac{d}{dx} \int_0^\delta \sigma\, r\, dy \qquad [61]$$

where the momentum area Ω is defined in Equation [32]. In terms of the displacement area Λ^*, defined in [10] and Ω, the shape parameter for axisymmetric flow is

$$h = \frac{\Lambda^*}{\Omega} \qquad [62]$$

The momentum equation, [61], will now be considered for the two cases where the boundary layer is thin compared to the radius of the body and where the boundary layer is of like magnitude.

BOUNDARY LAYER THIN RELATIVE TO BODY RADIUS: $\delta \ll r_w$

In the region forward of the tail, the boundary layer is thin relative to the radius of the body $\delta \ll r_w$. Here the momentum equation, [61], may be reduced to a simpler form. Since within the boundary layer

$$r_w \le r \le r_w + \delta \qquad [63].$$

it follows from [32] that

$$r_w\, \theta < \Omega < (r_w + \delta)\, \theta \qquad [34]$$

from [10] that

$$r_w\, \delta^* < \Lambda^* < (r_w + \delta)\, \delta^* \qquad [64]$$

and from [62]

$$\left(\frac{r_w}{r_w + \delta}\right) H < h < \left(\frac{r_w + \delta}{r_w}\right) H \qquad [65]$$

where H is the two-dimensional shape parameter

$$H = \frac{\delta^*}{\theta} \qquad [66]$$

Also

$$\frac{d}{dx}\left(r_w \int_0^\delta \sigma\, dy\right) < \frac{d}{dx} \int_0^\delta \sigma\, r\, dy < \frac{d}{dx}\left[(r_w + \delta) \int_0^\delta \sigma\, dy\right] \qquad [67]$$

Evidently for $\delta \ll r_w$, $\Omega = r_w\, \theta$, $\Lambda^* = r_w\, \delta^*$, $h = H$, and

$$\frac{d}{dx} \int_0^\delta \sigma\, r\, dy = \frac{d}{dx}\left(r_w \int_0^\delta \sigma\, dy\right)$$

Furthermore

$$\frac{d}{dx}\left(r_w \int_0^\delta \sigma\,dy\right) \cong r_w \frac{d}{dx} \int_0^\delta \sigma\,dy \qquad [68]$$

since $\left(\int_0^\delta \sigma\,dy\right)\frac{dr_w}{dx}$ is empirically of a lower order of magnitude. Hence the momentum

equation, [61], becomes for $\delta \ll r_w$

$$\frac{d(r_w\,\theta)}{dx} + (H + 2)\,\frac{r_w\,\theta}{U}\,\frac{dU}{dx} = r_w\left(\frac{\tau_w}{\rho\,U^2} + \frac{1}{\rho\,U^2}\,\frac{d}{dx}\int_0^\delta \sigma\,dy\right) \qquad [69]$$

The sum of terms $\dfrac{\tau_w}{\rho\,U^2}$ and $\dfrac{1}{\rho\,U^2}\,\dfrac{d}{dx}\displaystyle\int_0^\delta \sigma\,dy$ may be considered as an effective

coefficient of local skin friction, i.e.,

$$\left(\frac{\tau_w}{\rho\,U^2}\right)_{\mathrm{eff}} = \frac{\tau_w}{\rho\,U^2} + \frac{1}{\rho\,U^2}\,\frac{d}{dx}\int_0^\delta \sigma\,dy \qquad [70]$$

In their study of two-dimensional boundary layers in adverse pressure gradients, Wieghardt and Tillmann found that the values of $(\tau_w / \rho\,U^2)_{\mathrm{eff}}$ computed from the momentum changes of the mean flow displayed unexpected increases near separation.[31] Since tests by Ludwieg and Tillmann[32] have shown the values of $\tau_w / \rho\,U^2$ to decrease in an adverse pressure gradient faster than those for flat plates without pressure gradients, the explanation of the increase in $(\tau_w/\rho\,U^2)_{\mathrm{eff}}$ has to be sought elsewhere. Wieghardt has attributed this apparent increase wholly to the convergence of the flow caused by the thickening of the boundary layer on the opposite sides of the wind tunnel.[6,33] On the other hand, Newman[34] and various investigators of the National Advisory Committee for Aeronautics[35,36,37] have shown this increase to be partly accounted for by the increase in the value of the normal-stress term $\dfrac{1}{\rho\,U^2}\,\dfrac{d}{dx}\displaystyle\int_0^\delta \sigma\,dy$, especially close to separation. Hence for adverse pressure gradients, the decrease in the value of $\tau_w / \rho\,U^2$ tends to be compensated by the increase in the value of

$\dfrac{1}{\rho\,U^2}\,\dfrac{d}{dx}\displaystyle\int_0^\delta \sigma\,dy$. This makes the coefficient of local skin friction for flat plates without pressure gradient $(\tau_w / \rho\,U^2)_0$ a close approximation to the effective skin friction, at least for moderate pressure gradients. Lyon's experimental results tend to substantiate this.[27] Therefore with

$$\left(\frac{\tau_w}{\rho\,U^2}\right)_0 = \left(\frac{\tau_w}{\rho\,U^2}\right)_{\mathrm{eff}} \qquad [71]$$

Equation [69] becomes

$$\frac{d(\tau_w \theta)}{dx} + (H + 2) \frac{\tau_w \theta}{U} \frac{dU}{dx} = \tau_w \left(\frac{\tau_w}{\rho U^2}\right)_0 \qquad [72]$$

The coefficient of local skin friction for flat plates ($\tau_w / \rho U^2$)$_0$ decreases slowly with local Reynolds number R_θ. A suitable formula valid for a large range of Reynolds numbers is that derived in Reference 38 from the Kármán-Schoenherr formula for the total drag of flat plates,

$$\left(\frac{\tau_w}{\rho U^2}\right)_0 = \frac{0.01466}{\log_{10}(2R_\theta)\left[\frac{1}{2}\log_{10}(2R_\theta) + 0.4343\right]} \qquad [73]$$
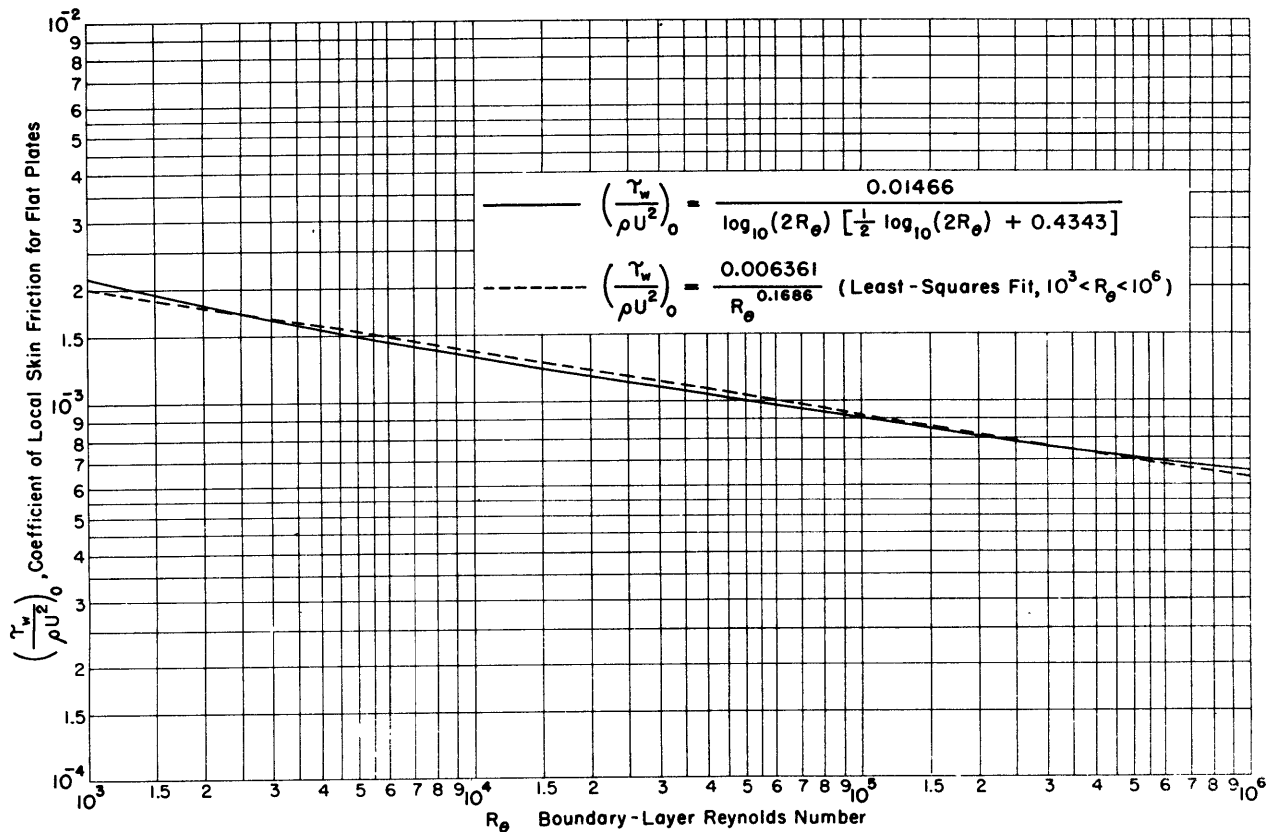
which is plotted in Figure 6.

Figure 6 - Local Skin Friction for Flat Plates as Function of Boundary-Layer Reynolds Number R_θ

A rapid procedure (and one sufficiently accurate for drag calculations) is to approximate ($\tau_w / \rho U^2$)$_0$ with a power law and to assume H constant. With

$$\left(\frac{\tau_w}{\rho U^2}\right)_0 = \frac{\zeta_0}{R_\theta^m} \qquad [74]$$

where m and ζ_0 are constants, [72] becomes

$$\frac{d(r_w\theta)}{dx} + \frac{(H+2)}{U}\frac{dU}{dx}(r_w\theta) = \left(\frac{r_w^{1+m}\zeta_0\,\nu^m}{U^m}\right)(r_w\theta)^{-m} \qquad [75]$$

which is a first-order differential equation in $r_w\theta$ of the Bernoulli type. For H constant, [75] gives for interval of integration x_1 to x_2

$$U_2^j\,(r_w\theta)_2^{1+m} = U_1^j\,(r_w\theta)_1^{1+m} + (1+m)\,\zeta_0\nu^m \int_{x_1}^{x_2} r_w^{1+m}\,U^{j-m}\,dx \qquad [76]$$

where

$$j \equiv (1+m)(H+2) \qquad [77]$$

Lyon found that $H = 1.4$ gave good agreement between the experimental and calculated drags.[27] Since $(\tau_w/\rho U^2)_0$ in Equation [73] gives almost a straight line on a log-log plot as shown in Figure 6, a power law approximation proves a close fit. For $10^3 < R_\theta < 10^6$, a least-squares fit of [73] gives

$$m = 0.1686$$
$$\zeta_0 = 0.006361$$
$$\qquad [78]$$

A more convenient nondimensional form of [76] is

$$\left(\frac{U}{U_\infty}\right)_2^j\left(\frac{r_w\theta}{L^2}\right)_2^{1+m} = \left(\frac{U}{U_\infty}\right)_1^j\left(\frac{r_w\theta}{L^2}\right)_1^{1+m} + \frac{(1+m)\,\zeta_0}{R_L^m}\int_{(l/L)_1}^{(l/L)_2}\left(\frac{r_w}{L}\right)^{1+m}\left(\frac{U}{U_\infty}\right)^{j-m}\sec\alpha\,d\!\left(\frac{l}{L}\right) \qquad [79]$$

BOUNDARY LAYER NEAR THE TAIL

It is apparent that the previous assumption $\delta \ll r_w$ is no longer valid towards the after end of the body where the radius r_w goes to zero at the tail and the boundary layer progressively thickens. Consequently the general form of the momentum equation [61] has to be employed; for constant h, it may be integrated to the form

$$\Omega_e = \Omega_g\left(\frac{U_g}{U_e}\right)^{h+2} + \frac{1}{U_e^{h+2}}\int_{x_g}^{x_e}\left(r_w\frac{\tau_w}{\rho U^2} + \frac{1}{\rho U^2}\frac{d}{dx}\int_0^\delta \sigma\,r\,dy\right)U^{h+2}\,dx \qquad [80]$$

where the subscript g refers to the initial point of integration and the subscript e to the tail of the body.

Experimental evidence[27] indicates that $r_w\dfrac{\tau_w}{\rho U^2} + \dfrac{1}{\rho U^2}\dfrac{d}{dx}\displaystyle\int_0^\delta \sigma\,r\,dy$ in the right-hand side of Equation [80] is substantially linear with respect to x along the after end, and drops to zero at the tail. Consequently

$$r_w \frac{\tau_w}{\rho U^2} + \frac{1}{\rho U^2} \frac{d}{dx} \int_0^\delta \sigma\, r\, dy = \left(r_w \frac{\tau_{w_0}}{\rho U^2}\right)_g \left(\frac{x_e - x}{x_e - x_g}\right) \qquad [81]$$

Furthermore, the variation of U with respect to x is also substantially linear along the after end or

$$\frac{U - U_e}{U_g - U_e} = \frac{x_e - x}{x_e - x_g} \qquad [82]$$

Inserting these linear relations, Equations [81] and [82], into momentum equation [80] gives

$$\Omega_e = \Omega_g \left(\frac{U_g}{U_e}\right)^{h+2} + \left(r_w \frac{\tau_{w_0}}{\rho U^2}\right)_g \frac{(x_e - x_g)}{(h + 3)(h + 4) U_e^{h+2} (U_g - U_e)^2}$$

$$\times \left[(h + 3) U_g^{h+4} - (h + 4) U_e U_g^{h+3} + U_e^{h+4}\right] \qquad [83]$$

or nondimensionally

$$\frac{\Omega_e}{L^2} = \frac{\Omega_g}{L^2}\left(\frac{U_g/U_\infty}{U_e/U_\infty}\right)^{h+2} + \left(\frac{r_w}{L}\right)_g\left(\frac{\tau_{w_0}}{\rho U^2}\right)_g \frac{\left[1 - \left(\frac{l}{L}\right)_g\right] \sec \alpha}{(h + 3)(h + 4)\left(\frac{U_e}{U_\infty}\right)^{h+2} \left(\frac{U_g}{U_\infty} - \frac{U_e}{U_\infty}\right)^2}$$

$$\times \left[(h + 3)\left(\frac{U_g}{U_e}\right)^{h+4} - (h + 4)\left(\frac{U_e}{U_\infty}\right)\left(\frac{U_g}{U_\infty}\right)^{h+3} + \left(\frac{U_e}{U_\infty}\right)^{h+4}\right] \qquad [84]$$

The initial position g of the tail portion of the boundary layer may be taken at 0.8 of the length of the body. An average value of $h = 1.4$ over the tail portion is appropriate in view of the value of $h_e = 1.42$ found on the Mark 13 Torpedo.[39]

In the region of the boundary layer near the tail, it is useful to establish relations between θ and Ω, δ^* and Λ^*, and h and H. A power law is assumed for the velocity profile or

$$\frac{u}{U} = \left(\frac{y}{\delta}\right)^n \qquad [85]$$

Substituting this expression into Equation [32] and performing the indicated integration results in

$$\Omega = r_w \, \theta \left\{ 1 + \left[\frac{H^2 \, (H+1)}{(H-1) \, (H+3)} \right] \left(\frac{\theta \, \cos \alpha}{r_w} \right) \right\} \qquad [86]$$

Also from Equation [10]

$$\Lambda^* = r_w \, \delta^* \left\{ 1 + \left[\frac{(H+1)^2}{2(H-1) \, (H+3)} \right] \left(\frac{\delta^* \cos \alpha}{r_w} \right) \right\} \qquad [87]$$

Furthermore,

$$h = H \left\{ \frac{1 + \left[\dfrac{H \, (H+1)^2}{2 \, (H-1) \, (H+3)} \right] \left(\dfrac{\theta \, \cos \alpha}{r_w} \right)}{1 + \left[\dfrac{H^2 \, (H+1)}{(H-1) \, (H+3)} \right] \left(\dfrac{\theta \, \cos \alpha}{r_w} \right)} \right\} \qquad [88]$$

In the wake where $r_w = 0$

$$h = \frac{H+1}{2} \qquad [89]$$

TURBULENT WAKE

The boundary layer leaving the tail of the body as the wake has a somewhat higher pressure and larger momentum area Ω_e than the wake far downstream. Since the momentum area Ω_∞ of the wake far downstream determines the drag of the body, a relation is required between Ω_∞ and the momentum area Ω_e of the boundary layer at the tail.

With no skin friction in the wake and with negligible effect from the normal-stress term the momentum equation [61] reduces to

$$\frac{d\Omega}{dx} + (h+2) \, \frac{\Omega}{U} \, \frac{dU}{dx} = 0 \qquad [90]$$

Integrating by parts over the length of the wake from the tail to infinity downstream yields

$$\Omega_\infty = \Omega_e \left(\frac{U_e}{U_\infty} \right)^{h_t + 2} \exp \left[\int_1^{h_e} \ln \frac{U_\infty}{U} \, dh \right] \qquad [91]$$

where the limiting value of h at infinity is unity.

The evaluation of $\exp \left[\int_1^{h_e} \ln \frac{U_\infty}{U} \, dh \right]$ proceeds empirically. Experimental evidence suggests an empirical fit of a higher order parabola of form

$$\frac{\ln \dfrac{U_\infty}{U}}{\ln \dfrac{U_\infty}{U_e}} = \left(\frac{h-1}{h_e - 1} \right)^q \qquad [92]$$
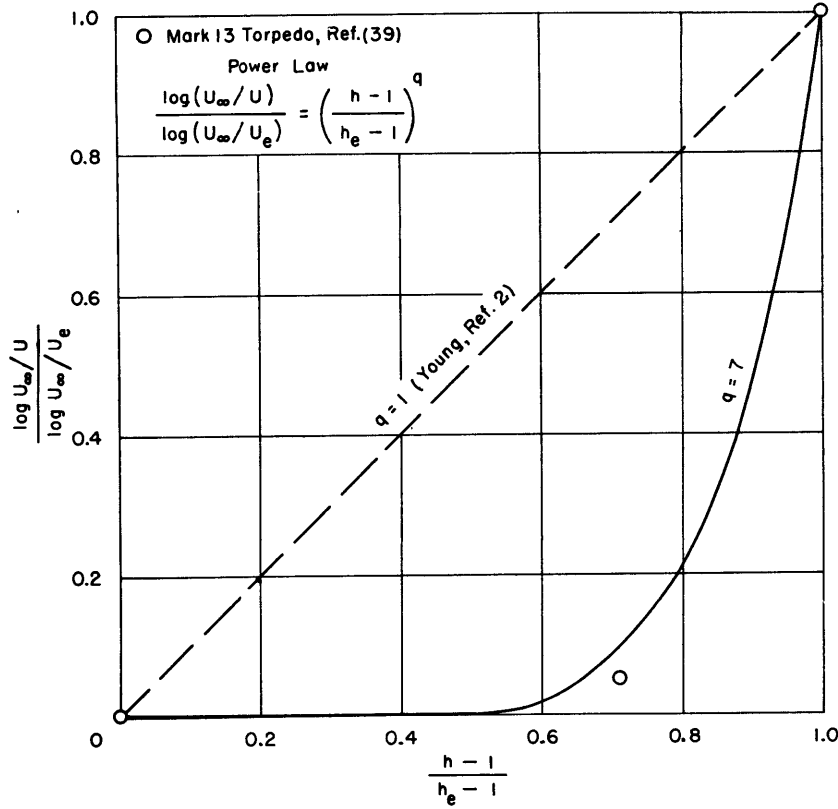
Figure 7 - Variation of Axisymmetric Shape Parameter h in Wake

Then

$$\int_1^{h_e} \ln \frac{U_\infty}{U} \, dh = \left(\frac{h_e - 1}{1 + q}\right) \ln \frac{U_\infty}{U_e} \qquad [93]$$

and

$$\exp\left[\int_1^{h_e} \ln \frac{U_\infty}{U} \, dh\right] = \left(\frac{U_e}{U_\infty}\right)^{\frac{1 - h_e}{1 + q}} \qquad [94]$$

Finally

$$\Omega_\infty = \Omega_e \left(\frac{U_e}{U_\infty}\right)^{\frac{(h_e + 2)\, q + 3}{1 + q}} \qquad [95]$$

This completes the relationships required for calculating the drag from the boundary-layer development. It is seen that both the momentum area and the shape parameter at the tail are required for a precise solution of the drag.

The choice of a value for q is not critical since a large difference in q results in only a small error in the drag. Considering only a very limited amount of two-dimensional data, Young[2] uses a linear relation for Equation [92], that is, a value of q of unity. As shown in Figure 7, test data for a body of revolution, the Mark 13 Torpedo,[39] though meager, indicate

that the ordinate $\dfrac{\ln U_\infty / U}{\ln U_\infty / U_t}$ approaches the limit of zero at the origin more gradually than by

a linear relationship. Until additional test data are available, it is suggested that a value of

$q = 7$ be used for drag calculations. If the value of $h_e = 1.42$ (from the data for the Mark 13

torpedo) is also used in Equation [95], there results finally

$$\Omega_\infty = \Omega_e \left(\frac{U_t}{U_\infty}\right)^{3.38}$$ [96]

CONCLUDING REMARKS

The method described in this report gives a relatively simple procedure for computing the viscous drag of a body of revolution to an engineering degree of accuracy. Any marked deviation between the calculated and measured values of drag should be expected only in the case of a shape differing radically from the usual streamlined figure.

To test the method of this report, drag coefficients of the model of the airship AKRON were computed at various Reynolds numbers for comparison with measured values.[40,41] Measured values of the pressure distribution and measured locations of the transition point were used in the calculations. The computed values were found to lie between the measured values as shown in the accompanying table.

TABLE 2

Comparison of Measured and Computed Values of Drag Coefficient of
1/40-Scale Model of Airship AKRON

Reynolds Number R_L	Drag Coefficient C_D		
	Experimental		Computed
	Wooden Model	Metal Model	
12.3×10^6	0.0198	0.0228	0.0222
15.0×10^6	0.0193	0.0223	0.0216
17.3×10^6	0.0190	0.0219	0.0211

In conclusion, it is noted that in the case of low Reynolds numbers the viscous drag of bodies of revolution depends to a large measure on the position of transition, and that in the case of high Reynolds numbers, it depends on the detailed development of the turbulent boundary layer in pressure gradients. The current theories on turbulent flow are semi-empirical in nature. Accordingly, before all the processes determining viscous drag are fully elucidated, there is need for accurate measurements of such factors as velocity profiles and shearing-stress profiles in turbulent boundary layers especially at high Reynolds numbers.

For convenient reference, the various steps involved in calculating the viscous drag are summarized in Appendix I.

ACKNOWLEDGMENTS

REFERENCES

1. Shvets, M.E., "Method of Successive Approximations for the Solution of Certain Problems in Aerodynamics," NACA TM 1286, April 1951 (Translation from Prikladnaya Matematika i Mekhanika, Vol. 13, No. 3, 1949).

2. Young, A.D., "The Calculation of the Total and Skin Friction Drags of Bodies of Revolution at Zero Incidence," (British) Aeronautical Research Committee R & M 1874, April 1939.

3. Landweber, L., "The Axially Symmetric Potential Flow About Elongated Bodies of Revolution," TMB Report 761, August 1951.

4. Young, A.D. and Owen, P.R., "A Simplified Theory for Streamline Bodies of Revolution and its Application to the Development of High-Speed Shapes," (British) Aeronautical Research Committee R & M 2071, July 1943.

5. Goldstein, S., (ed), "Modern Developments in Fluid Dynamics," Clarendon Press (Oxford), 1938.

6. Tollmien, W., (ed.) "Boundary Layers," (British) Ministry of Supply VG R & T 1001-1006, March 1948 (Translation of AVA Monographs).

7. Schlichting, H., "Grenschicht-Theorie" (Boundary-Layer Theory), Verlag G. Braun (Karlsruhe), 1951.

8. Millikan, C.B., "The Boundary Layer and Skin Friction for a Figure of Revolution," Trans. ASME, APM-54-3, 1932.

9. Thwaites, B., "Approximate Calculation of the Laminar Boundary Layer," Aeronautical Quarterly, Vol. 1, Part 3, November 1949.

10. Rott, N. and Crabtree, L.F., "Simplified Laminar Boundary-Layer Calculations for Bodies of Revolution and for Yawed Wings," Jour. Inst. Aero. Sci., Vol. 19, No. 8, August 1952.

11. Tollmien, W. "The Production of Turbulence," NACA TM 609, March 1931. (Translation from Nachrichten der Gesellschaft der Wissenschaften zu Göttingen Mathematisch-Physikalische Klasse, 1929.)

12. Chiarulli, P. and Freeman, J.C., "Stability of the Boundary-Layer," Monograph VI, Air Materiel Command (Wright-Patterson Air Force Base, Dayton, Ohio), August 1948.

13. Schubauer, G.B. and Skramstad, H.K., "Laminar-Boundary-Layer Oscillations and Transition on a Flat Plate," NACA Report 909, 1948.

14. Liepmann, H.W., "Investigations on Laminar Boundary-Layer Stability and Transition on on Curved Boundaries," NACA Wartime Report W-107, August 1943.

15. Taylor, G.I., "Some Recent Developments in the Study of Turbulence," Proceedings of the Fifth International Congress for Applied Mechanics, Cambridge, Mass., 1939.

16. Schubauer, G.B., "Airflow in the Boundary Layer of an Elliptic Cylinder," NACA Report 652, 1939.

17. Liepmann, H.W., "Investigation of Boundary Layer Transition on Concave Walls," NACA Wartime Report W-87, February 1945.

18. Bursnall, W.J. and Loftin, L.K., Jr., "Experimental Investigation of Laminar-Boundary-Layer Separation," NACA TN 2338, April 1951.

19. Liepmann, H.W. and Fila, G.H., "Investigations of Effects of Surface Temperature and Single Roughness Elements on Boundary-Layer Transition," NACA Report 890, 1947.

20. Jones, B.M., "Flight Experiments on the Boundary Layer," Jour. Aero. Sci., Vol. 5, No. 3, January 1938.

21. Mangler, W., "Boundary Layers on Bodies of Revolution in Symmetric Flow," Joint Intelligence Objectives Agency, Washington, D.C. BIGS-13, June 1946; also Goodyear Aircraft Company, Report 45-A17, 1945. (Translation from AVA Report 45/A/17, 1945).

22. Schlichting, J. and Ulrich, A., "Zur Berechnung des Umschlages Laminar-Turbulenten" (On the Calculation of Laminar-Turbulent Transition), Jahrbuch 1942 der deutschen Luftfahrtforschung.

23. Oudart, A., "Le Calcul de la Couche Limite Laminaire ou Turbulente en Fluide Compressible; Les Methodes Semi-Empiriques Modernes et Les Travaux du Dr. Ing. Alfred Walz," (The Calculation of the Laminar or Turbulent Boundary in a Compressible Fluid; The Modern Semi-Empirical Methods and Work of Dr. Alfred Walz), Publications Scientifiques et Techniques du Ministère de l'Air, Paris, No. 223, 1949.

24. Zalovcik, J.A. and Skoog, R.B., "Flight Investigation of Boundary-Layer Transition and Profile Drag of an Experimental Low-Drag Wing Installed on a Fighter-Type Airplane," NACA Wartime Report L-94, April 1945.

25. Von Doenhoff, A.E., "Investigation of the Boundary Layer About a Symmetrical Airfoil in a Wind Tunnel of Low Turbulence," NACA Wartime Report L-507, August 1940.

26. Braslow, A.L. and Visconti, F., "Investigation of Boundary-Layer Reynolds Number for Transition on an NACA $65_{(215)}$-114 Airfoil in the Langley Two-Dimensional Low-Turbulence Pressure Tunnel," NACA TN 1704, October 1948.

27. Lyon, H.M., "A Study of the Flow in the Boundary Layer of Streamline Bodies," (British) Aeronautical Research Committee R & M 1622, May 1934.

28. Dryden, H.L., "Air Flow in the Boundary Layer Near a Plate," NACA Report 562, 1936.

29. Hall, A.A. and Hislop, G.S., "Experiments on the Transition of the Laminar Boundary Layer on a Flat Plate," (British) Aeronautical Research Committee, R & M 1843, August 1938.

30. Chou, P.Y., "On an Extension of Reynolds' Method of Finding Apparent Stress and the Nature of Turbulence," Chinese Journal of Physics, Vol. 4, No. 1, June 1940.

31. Wieghardt, K. and Tillmann, W., "On the Turbulent Friction Layer for Rising Pressure," NACA TM 1314, October 1951 (Translation of ZWB Untersuchungen und Mitteilungen 6617, November 1944).

32. Ludwieg, H. and Tillmann, W., "Investigations of Surface Shearing Stresses in Turbulent Boundary Layers," NACA TM 1285, May 1950. (Translated from Ingenieur-Archiv, Vol. 17, No. 4, 1949.)

33. Wieghardt, K., "Some Remarks on Turbulent Boundary Layers in Two and Three Dimensional Flow," Admiralty Research Laboratory (Teddington) Report ARL/R1/G/HY/12/1, October 1950.

34. Newman, B.G., "Skin Friction in a Retarded Turbulent Boundary Layer Near Separation," (Australian) Department of Supply, Aeronautical Research Laboratories Report A.73, November 1950.

35. Rubert, K.F. and Persh, J., "A Procedure for Calculating the Development of Turbulent Boundary Layers under the Influence of Adverse Pressure Gradients," NACA TN 2478, September 1951.

36. Goldschmied, F.R., "Skin Friction of Incompressible Turbulent Boundary Layers under Adverse Pressure Gradients," NACA TN 2431, August 1951.

37. Bidwell, J.M., "Application of the von Kármán Momentum Theorem to Turbulent Boundary Layers," NACA TN 2571, December 1951.

38. Granville, P.S., "A Method for the Calculation of the Turbulent Boundary Layer in a Pressure Gradient," TMB Report 752, May 1951.

39. Eggers, H.A., "Wake Survey of the Mark 13 Torpedo," TMB Report 583, July 1947.

40. Freeman, H.B., "Measurements of Flow in the Boundary Layer of a 1/40-Scale Model of the U.S. Airship AKRON," NACA Report 430, 1932.

41. Freeman, H.B., "Force Measurements on a 1/40-Scale Model of the U.S. Airship AKRON," NACA Report 432, 1932.

APPENDIX 1

CALCULATION PROCEDURE

For convenient reference, the various steps for computing the viscous drag of bodies of revolution in axisymmetric flow are listed here.

1. **Prescribed Data**

   a. **Profile dimensions**

   $$\frac{r_w}{L}, \quad \alpha = f\left(\frac{l}{L}\right)$$

   b. **Pressure distribution**

   $$\frac{p - p_\infty}{\frac{1}{2} \rho U_\infty^2} = 1 - \left(\frac{U}{U_\infty}\right)^2 = f\left(\frac{l}{L}\right) \tag{8}$$

   c. **Body Reynolds number**

   $$R_L = \frac{U_\infty L}{\nu} \tag{38}$$

2. **Transition Point**

   a. **Neutral stability point** $\left(\frac{l}{L}\right)_N$

   (1) $R_\theta = f\left(\frac{l}{L}\right)$ is computed from

   $$\frac{R_\theta^2}{R_L} = \frac{4}{9} \frac{1}{\left(\frac{U}{U_\infty}\right)^4 \left(\frac{r_w}{L}\right)^2} \int_0^{l/L} \left(\frac{U}{U_\infty}\right)^5 \left(\frac{r_w}{L}\right)^2 \sec \alpha \, d\left(\frac{l}{L}\right) \tag{51}$$

   (2) $\frac{\theta^2}{\nu} \frac{dU}{dx} = f\left(\frac{l}{L}\right)$ is computed from

   $$\frac{\theta^2}{\nu} \frac{dU}{dx} = \left(\frac{R_\theta^2}{R_L}\right) \frac{1}{\left(\frac{U}{U_\infty}\right)^2} \frac{d\left(\frac{U}{U_\infty}\right)}{d\left(\frac{l}{L}\right)} \cos \alpha \tag{52}$$

   (3) $R_\theta = f\left(\frac{\theta^2}{\nu} \frac{dU}{dx}\right)$ is plotted to intersect the neutral stability curve of Figure 3

   to give $\left(\frac{l}{L}\right)_N$

   b. **Self-excited transition point** $\left(\frac{l}{L}\right)_{ts}$

(1) $\overline{\dfrac{\tilde{\theta}^2}{\nu}\dfrac{d\tilde{U}}{d\tilde{x}}} = f\left(\dfrac{l}{L}\right)_{ts}$ is computed for various assumed values of $\left(\dfrac{l}{L}\right)_{ts}$ from

$$\overline{\frac{\tilde{\theta}^2}{\nu}\frac{d\tilde{U}}{d\tilde{x}}} = \frac{4}{45} - \frac{1}{5}\left\{\frac{\left[\dfrac{\left(\dfrac{R_\theta{}^2}{R_L}\right)\left(\dfrac{r_w}{L}\right)^2}{\left(\dfrac{U}{U_\infty}\right)}\right]_{ts} - \left[\dfrac{\left(\dfrac{R_\theta{}^2}{R_L}\right)\left(\dfrac{r_w}{L}\right)^2}{\left(\dfrac{U}{U_\infty}\right)}\right]_N}{\displaystyle\int_{(l/L)_N}^{(l/L)_{ts}}\left(\dfrac{r_w}{L}\right)^2 \sec\alpha\, d\left(\dfrac{l}{L}\right)}\right\} \qquad [53]$$

(2) $R_{\theta,ts} - R_{\theta,N} = f\left(\overline{\dfrac{\tilde{\theta}^2}{\nu}\dfrac{d\tilde{U}}{d\tilde{x}}}\right)$ is plotted to intersect the curve of Figure 4 to give

correct value of $\left(\dfrac{l}{L}\right)_{ts}$

c. Transition point for free-stream turbulence $\left(\dfrac{l}{L}\right)_{tb}$

(1) For prescribed $\dfrac{\sqrt{\overline{u'^2}}}{U_\infty}$ of free stream $\left(R_{\theta,tb} - R_{\theta,N}\right)_0$ is determined from Figure 5.

(2) $R_{\theta,tb}$ is determined from

$$\frac{R_{\theta,tb} - R_{\theta,N}}{R_{\theta,ts} - R_{\theta,N}} = \left(\frac{R_{\theta,tb} - R_{\theta,N}}{R_{\theta,ts} - R_{\theta,N}}\right)_0 \qquad [54]$$

3. Laminar Boundary Layer

$\left(\dfrac{\Omega}{L^2}\right)_t$ at transition point $\left(\dfrac{l}{L}\right)_t$ is computed from

$$\left(\frac{\Omega}{L^2}\right)_t^2 = \left(\frac{r_w\,\theta}{L^2}\right)_t^2 = \frac{4}{9}\frac{1}{R_L\left(\dfrac{U}{U_\infty}\right)^6}\int_0^{(l/L)_t}\left(\frac{r_w}{L}\right)^2\left(\frac{U}{U_\infty}\right)^5\sec\alpha\, d\left(\frac{l}{L}\right) \qquad [36]$$

or if $R_\theta = f\left(\dfrac{l}{L}\right)$ has been computed

$$\left(\frac{\Omega}{L^2}\right)_t = \left(\frac{r_w\,\theta}{L^2}\right)_t = \left(\frac{R_\theta}{R_L}\right)_t\frac{\left(\dfrac{r_w}{L}\right)_t}{\left(\dfrac{U}{U_\infty}\right)_t}$$

4. Turbulent Boundary Layer

a. Thin boundary layer, $\delta \ll r_w$

$\dfrac{\Omega}{L^2} = \dfrac{r_w\,\theta}{L^2}$ is computed over distance $\left(\dfrac{l}{L}\right)_t$ to $\left(\dfrac{l}{L}\right) = 0.8$ from

$$\left(\frac{U}{U_\infty}\right)_{0.8}^{j}\left(\frac{r_w\,\theta}{L^2}\right)_{0.8}^{1+m} = \left(\frac{U}{U_\infty}\right)_{t}^{j}\left(\frac{r_w\,\theta}{L^2}\right)_{t}^{1+m}$$

$$+\ \frac{(1+m)\,\zeta_0}{R_L{}^m}\ \int_{(l/L)_t}^{0.8}\left(\frac{r_w}{L}\right)^{1+m}\left(\frac{U}{U_\infty}\right)^{j-m}\ \sec\alpha\ \ d\left(\frac{l}{L}\right)$$

[79]

where $m = 0.1686$

$j = 3.9732$

$\zeta_0 = 0.006361$

b. Boundary layer near tail

(1) $\left(\dfrac{\Omega}{L^2}\right)_e$ is computed from

$$\left(\frac{\Omega}{L^2}\right)_e = \left(\frac{\Omega}{L^2}\right)_g\left(\frac{U_s/U_\infty}{U_t/U_\infty}\right)^{h+2}$$

$$+\left(\frac{r_w}{L}\right)_g\left(\frac{\tau_{w_0}}{\rho\,U^2}\right)_g\ \frac{\left(1-\dfrac{l_g}{L}\right)\ \sec\alpha}{(h+3)\,(h+4)\left(\dfrac{U_t}{U_\infty}\right)^{h+2}\left(\dfrac{U_s}{U_\infty}-\dfrac{U_t}{U_\infty}\right)^{2}}$$

[84]

$$\times\left[(h+3)\left(\frac{U_g}{U_e}\right)^{h+4} - (h+4)\left(\frac{U_e}{U_\infty}\right)\left(\frac{U_g}{U_\infty}\right)^{h+3} + \left(\frac{U_e}{U_\infty}\right)^{h+4}\right]$$

(2) A value of $h = 1.4$ and $\left(\dfrac{l}{L}\right)_g = 0.8$ is to be used.

5. Wake

Ω_∞ is computed from

$$\Omega_\infty = \Omega_e \left(\frac{U_e}{U_\infty}\right)^{3.38}$$

[96]

6. Viscous Drag

Drag coefficient C_D is computed from

$$C_D = \frac{4\pi\Omega_\infty}{A}$$

[7]

INITIAL DISTRIBUTION

Copies

20	Chief, Bureau of Ships, Technical Library (Code 3 27), for distribution:
	5 Technical Library
	1 Technical Assistant to Chief of Bureau (Code 106)
	3 Research (Code 3 00)
	2 Applied Science (Code 370)
	2 Design (Code 410)
	3 Preliminary Design (Code 420)
	3 Submarines (Code 515)
	1 Propellers and Shafting (Code 554)

5 Chief, Bureau of Ordnance, Underwater Ordnance (Re6a)
    1 Dr. A. Miller

3 Chief, Bureau of Aeronautics, for distribution:
    2 Aerodynamics and Hydrodynamics Branch (DE-3)
    1 Applied Mathematics Branch

4 Chief of Naval Research, for distribution:
    2 Fluid Mechanics (N 426)
    1 Undersea Warfare (466)
    1 Mathematics (432)

2 Director, U.S. Naval Research Laboratory, Washington 25, D.C.

4 Commander, U.S. Naval Ordnance Laboratory, Mechanics Division, White Oak, Silver Spring 19, Md.

2 Commander, U.S. Naval Ordnance Test Station, Inyokern, China Lake, Calif.
    1 Underwater Ordnance Division, Pasadena Annex, 3202 E. Foothill Blvd., Pasadena 8, Calif.

1 Commander, Mare Island Naval Shipyard, Vallejo, Calif.

1 Commander, Norfolk Naval Shipyard, Portsmouth, Va.

1 Commander, Portsmouth Naval Shipyard, Portsmouth, N.H.

1 Commander, U.S. Naval Proving Ground, Dahlgren, Va.

1 Commanding Officer and Director, U.S. Navy Underwater Sound Laboratory, Fort Trumbull, New London, Conn.

2 Commanding Officer, U.S. Naval Underwater Ordnance Station, Design Section, Newport, R.I.

1 Commanding Officer, U.S. Naval Air Test Center, Patuxent River, Md.

1 Superintendent, U.S. Naval Post Graduate School, Monterey, Calif.

1 Director, Marine Physical Laboratory, U.S. Navy Electronics Laboratory, San Diego 52, Calif.

1 Chairman, Research and Development Board, Dept. of Defense Bldg., Washington 25, D.C.

Copies

1	Library of Congress, Technical Information Division, Washington 25, D.C.
2	Chief, Service Division, The Armed Services Technical Information Agency, Document Service Center, Knott Building, 4th and Main Sts., Dayton 2, Ohio
1	Commanding Officer, Frankford Arsenal, Philadelphia 37, Pa.
1	Director, Ballistic Research Laboratory, Aberdeen Proving Ground, Aberdeen, Md.
1	Director, Technical Information Branch, Aberdeen Proving Ground, Aberdeen, Md.
1	Director, National Advisory Committee for Aeronautics, 1724 F St., N.W., Washington 25, D.C.
1	Director, Langley Aeronautical Laboratory, Langley Air Force Base, Va.
1	Director, Lewis Flight Propulsion Laboratory, Cleveland Airport, Cleveland 11, Ohio
1	Director, Ames Aeronautical Laboratory, Moffett Field, Mountain View, Calif.
1	Director, Oak Ridge National Laboratory, P.O. Box P, Oak Ridge, Tenn.
1	Chief, National Hydraulic Laboratory, National Bureau of Standards, Washington 25, D.C.
1	Hydrodynamic Laboratory, Attn: Executive Committee, California Institute of Technology, 1201 E. California St., Pasadena 4, Calif.
1	Director, Institute of Engineering Research, University of California, Berkeley 4, Calif.
1	Director, Fluid Mechanics Laboratory, University of California, Berkeley 4, Calif.
1	Director, Hydraulic Laboratory, Carnegie Institute of Technology, Pittsburgh 13, Pa.
1	Director, Hydraulic Laboratory, Colorado University, Boulder, Colo.
1	Director, Fluid Mechanics Laboratory, Columbia University, New York 27, N.Y.
1	Director, Hydraulic Research Laboratory, University of Connecticut, Box U-37, Storrs, Conn.
1	Director, Iowa Institute of Hydraulic Research, State University of Iowa, Iowa City, Iowa
1	Director, Applied Physics Laboratory, Johns Hopkins University, 8621 Georgia Ave., Silver Spring, Md.
1	Director, Institute for Fluid Dynamics and Applied Mathematics, University of Maryland, College Park, Md.
1	Director, Experimental Naval Tank, Department of Naval Architecture and Marine Engineering, University of Michigan, Ann Arbor, Mich.
1	Director, Experimental Towing Tank, Stevens Institute of Technology, 711 Hudson St., Hoboken, N.J.

Copies

1   Director, St. Anthony Falls Hydraulic Laboratory, University of Minnesota, Minneapolis 14, Minn.

1   Director, Engineering and Industrial Research Station, Mississippi State College, State College, Miss.

1   Director, Fluid Mechanics Laboratory, New York University, New York 53, N.Y.

1   Director, Robinson Hydraulic Laboratory, Ohio State University, Columbus 10, Ohio

1   Director, Hydraulic Laboratory, Pennsylvania State College, State College, Pa.

1   Director, Ordnance Research Laboratory, Pennsylvania State College, State College, Pa.

1   Director, Engineering Experiment Station, University of Tennessee, Knoxville 16, Tenn.

1   Director, Engineering Experiment Station, Utah State Agricultural College, Logan, Utah

1   Director, Hydraulic Laboratory, University of Washington, Seattle 5, Wash.

1   Director, Hydraulic Laboratory, University of Wisconsin, Madison 6, Wis.

1   Director, Alden Hydraulic Laboratory, Worcester Polytechnic Institute, Worcester 2, Mass.

1   Director, Midwest Research Institute, 4049 Pennsylvania, Kansas City 2, Mo.

1   Director of Research, The Technological Institute, Northwestern University, Evanston, Ill.

1   Administrator, Webb Institute of Naval Architecture, Crescent Beach Road, Glen Cove, Long Island, N.Y.

1   Chairman, Department of Aeronautical Engineering, New York University, New York 53, N.Y.

1   Head, Department of Aeronautical Engineering, Pennsylvania State College, State College, Pa.

1   Head, Department of Aeronautical Engineering, Georgia Institute of Technology, Atlanta, Ga.

1   Head, Department of Aeronautical Engineering and Applied Mechanics, Polytechnic Institute of Brooklyn, 99 Livingston St., Brooklyn 2, N.Y.

1   Head, Aeronautical Engineering Department, Catholic University, Washington, D.C.

1   Head, Department of Aeronautical Engineering, John Hopkins University, Baltimore 18, Md.

1   Head, Department of Naval Architecture and Marine Engineering, Massachusetts Institute of Technology, Cambridge 39, Mass.

Copies

1	Reed Research, Inc., 1048 Potomac St., N.W., Washington, D.C.
2	Supervisor of Shipbuilding and Navy Inspector of Ordnance, General Dynamics Corporation, Electric Boat Division, Groton, Conn.
2	Newport News Shipbuilding and Dry Dock Company, Newport News, Va.
	1 Senior Naval Architect
	1 Supervisor, Hydraulics Laboratory
1	Director, Applied Physics Division, Sandia Laboratory, Albuquerque, N.M.
1	Director of Research, Vickers Incorporated, Detroit, Mich.
1	Editor, Aeronautical Engineering Review, 2 E. 64th St., New York 21, N.Y.
1	Editor, Applied Mechanics Review, Midwest Research Institute, 4049 Pennsylvania, Kansas City 2, Mo.
1	Editor, Bibliography of Technical Reports, Office of Technical Services, U.S. Department of Commerce, Washington 25, D.C.
1	Editor, Engineering Index, 29 W. 39th St., New York 18, N.Y.
1	Editor, Mathematical Reviews, Brown University, Providence, R.I.
1	Librarian, American Society of Civil Engineers, 33 W. 39th St., New York 18, N.Y.
1	Librarian, American Society of Mechanical Engineers, 29 W. 39th St., New York 18, N.Y.
1	Librarian, Institute of the Aeronautical Sciences, 2 E. 64th St., New York 21, N.Y.
1	Librarian, Pacific Aeronautical Library, Institute of the Aeronautical Sciences, 7660 Beverly Blvd., Los Angeles 36, Calif.
1	Librarian, Stanford University Libraries, Stanford, Calif.
1	Librarian, Rensselear Polytechnic Institute, Troy, N.Y.
1	Librarian, Towne Scientific School, University of Pennsylvania, Philadelphia 4, Pa.
1	Librarian, Illinois Institute of Technology, 3300 Federal St., Chicago 16, Ill.
1	Librarian, Franklin Institute, Parkway at 20th St., Philadelphia, Pa.
1	Librarian, College of Engineering, Cornell University, Ithaca, N.Y.
1	Librarian, Case Institute of Technology, Cleveland 6, Ohio
1	Librarian, Carnegie Institute of Technology, Pittsburgh 13, Pa.
1	Librarian, Daniel Guggenheim Aeronautical Laboratory, California Institute of Technology, Pasadena 4, Calif.
1	Technical Library, Douglas Aircraft Co., Inc., El Segundo, Calif.
1	Technical Library, Cornell Aeronautical Laboratory, Cornell Research Foundation, Box 235, Buffalo 21, N.Y.

Copies

1	Technical Library, Consolidated Vultee Aircraft Corporation, San Diego 12, Calif.
1	Technical Library, Glenn L. Martin Co., Baltimore 3, Md.
1	Technical Library, Grumann Aircraft Engineering Corporation, Bethpage, Long Island, N.Y.
1	Technical Library, Lockheed Aircraft Corporation, 2555 N. Hollywood Way, Burbank, Calif.
1	Technical Library, McDonnell Aircraft Corporation, Box 516, St. Louis 3, Mo.
1	Technical Library, North American Aviation, Inc., 12241 Lakewood Blvd., Downey, Calif.
1	Technical Library, North American Aviation, Inc., El Segundo, Calif.
1	Technical Library, Northrop Aircraft Co., 1017 E. Broadway, Hawthorne, Calif.
1	Technical Library, Pratt and Whitney Aircraft Division, United Aircraft Corp., East Hartford 8, Conn.
1	Engineering Library, Curtiss-Wright Corporation, Propeller Division, Caldwell, N.J.
1	Prof. M. Abkowitz, Department of Naval Architecture and Marine Engineering, Massachusetts Institute of Technology, Cambridge 39, Mass.
1	Prof. R.C. Binder, Department of Mechanical Engineering, Purdue University, Lafayette, Ind.
1	Prof. G. Birkhoff, Harvard University, Cambridge, Mass.
1	Mr. R. Bond, Research Engineer, University of California, Berkeley 4, Calif.
1	Mr. J.P. Breslin, Gibbs and Cox, 21 West St., New York 6, N.Y.
1	Dr. G. Carrier, School of Engineering, Harvard University, Cambridge, Mass.
1	Dr. E.P. Cooper, Naval Ordnance Test Station, Pasadena Annex, 3202 E. Foothill Blvd., Pasadena 8, Calif.
1	Dr. A.E. von Doenhoff, Langley Aeronautical Laboratory, Langley Air Force Base, Va.
1	Dr. H. Emmons, School of Engineering, Harvard University, Cambridge, Mass.
1	Dr. F.N. Frenkiel, Applied Physics Laboratory, Johns Hopkins University, 8621 Georgia Avenue, Silver Spring, Md.
1	Dr. D. Gilbarg, Department of Mathematics, Indiana University, Bloomington, Ind.
1	Prof. W.S. Hamilton, Technological Institute, Northwestern University, Evanston, Ill.
1	Prof. C.W. Harris, Department of Civil Engineering, University of Washington, Seattle 5, Wash.

Copies

1	Prof. A.D. Hay, Princeton University, Princeton, N.J.
1	Dr. S. Hoerner, Gibbs and Cox, 21 West St., New York 6, N.Y.
1	Dr. A. Kantrowitz, Cornell University, Ithaca, N.Y.
1	Dr. C. Kaplan, Langley Aeronautical Laboratory, Langley Air Force Base, Va.
1	Dr. Th. von Kármán, 1051 S. Marengo St., Pasadena, Calif.
1	Mr. J. Kotik, c/o Prof. G. Birkhoff, Harvard University, Cambridge, Mass.
1	Dr. L.S.G. Kovasznay, Department of Aeronautics, Johns Hopkins University, Baltimore 18, Md.
1	Dr. P. Lagerstrom, GALCIT, California Institute of Technology, Pasadena 4, Calif.
1	Prof. E.V. Laitone, University of California, Berkeley 4, Calif
1	Mr. C.A. Lee, Hydraulic Engineer, Research and Development Laboratories, Kimberly-Clark Corporation, Neenah, Wis.
1	Dr. H. Liepmann, GALCIT, California Institute of Technology, Pasadena 4, Calif.
1	Dr. C.C. Lin, Department of Mathematics, Massachusetts Institute of Technology, Cambridge 39, Mass.
1	Prof. J.W. Miles, University of California, Los Angeles, Calif.
1	Dr. Max Munk, U.S. Naval Ordnance Laboratory, White Oak, Silver Spring 19, Md.
1	Prof. C.J. Peirce, Headquarters, USAFE, APO 633, c/o Postmaster, New York, N.Y.
1	Dr. W. Pell, Department of Mathematics, University of Kentucky, Lexington, Ky.
1	Dr. M.S. Plesset, California Institute of Technology, Pasadena 4, Calif.
1	Dr. V.L. Schiff, Stanford University, Stanford, Calif.
1	Dr. K.E. Schoenherr, School of Engineering, Notre Dame University, Notre Dame, Ind.
1	Dr. G.B. Schubauer, National Bureau of Standards, Washington, D.C.
1	Prof. W. Sears, Graduate School of Engineering, Cornell University, Ithaca, N.Y.
1	Prof. R.A. Seban, Department of Mechanical Engineering, University of California, Berkeley 4, Calif.
1	Prof. F.B. Seely, Fluid Mechanics and Hydraulics Laboratory, University of Illinois, Urbana, Ill.
1	Mr. N. Tetervin, Langley Aeronautical Laboratory, Langley Air Force Base, Va.
1	Prof. L. Troost, Head, Department of Naval Architecture and Marine Engineering, Massachusetts Institute of Technology, Cambridge 39, Mass

Copies

1	Dr. C.A. Truesdell, Department of Mathematics, University of Indiana, Blooming-ton, Ind.
1	Prof. J. Vennard, Department of Civil Engineering, Stanford University, Stanford, Calif.
1	Prof. A. Weinstein, Department of Mathematics, University of Maryland, College Park, Md.
1	Prof. John R. Weske, Mechanical Engineering Department, Johns Hopkins University, Baltimore 18, Md.
1	Dr. G.F. Wislicenus, Mechanical Engineering Department, Johns Hopkins University, Baltimore 18, Md.
1	Prof. C. Yih, Department of Civil Engineering, Colorado A and M College, Fort Collins, Colo.
1	Australian Council for Aeronautics, Box 4331 G.P., Melbourne, Australia
1	Dr. F.C. Roesler, Physikalisches Institut, Technische Hochschule Graz, Rechbauerstrasse 12, Graz, Austria
1	Dr. G.N. Patterson, Institute of Aerophysics, University of Toronto, Toronto 5, Canada
8	U.S. Naval Attaché, U.S. Naval Attaché for Air, London, England
1	Head, Aerodynamics Division, National Physical Laboratory, Teddington, Middlesex, England
1	Head, Aerodynamics Department, Royal Aircraft Establishment, Farnborough, Hants, England
1	Head, College of Aeronautics, Cranfield, Bletchley, Bucks, England
1	Head, Aeronautics Department, Imperial College, London S.W. 7, England
1	Editor, Index Aeronauticas, Ministry of Supply, Millbank, London, S.W. 1, England
1	Editor, Physics Abstracts, Institution of Electrical Engineers, Savoy Place, London W.C. 2, England
1	Prof. G.K. Batchelor, Trinity College, Cambridge University, Cambridge, England
1	Dr. F. Ursell, Trinity College, Cambridge, England
1	Prof. J. Howarth, Department of Mathematics, University of Bristol, Bristol, England
1	Dr. S.L. Smith, Director, British Shipbuilding Research Association, 5 Chester-field Gardens, Curzon St., London W.1, England
1	Sir R.V. Southwell, 9 Lathburg Road, Oxford, England
1	Prof. K. Stewartson, Department of Mathematics, University of Bristol, Bristol, England

Copies

1	Dr. Vandry, Admiralty Research Laboratory, Teddington, England
1	Directeur du Bassin d'Essais Des Carénes 6, Boulevard Victor, Paris XV, France
1	Directeur, Laboratoire Dauphinois d'Hydraulique des Ateliers Neyrpic, Avenue de Beauvert, Grenoble (Isére), France
1	Office, National d'Études et de Recherches Aéronautique 3, rue Léon Bonnat, Paris XVI, France
1	Dr. J. Dieudonné, Directeur, Institut de Recherches de la Construction Navale, 1 Boulevard Haussmann, Paris (9e), France
1	Prof. J. Kampé de Fériet, Faculté des Sciences, Université de Lille, Lille (Nord), France
2	O.N. ERA, Service des Relations Extérieures et de la Documentation, 25-39, Avenue de la Division-Leclerc, Chatillon-sous-Bagneux (Seine), France
1	Prof. D.P. Riabouchinsky, Centre National de la Recherche Scientifique, 13 Quai d'Orsay, Paris VII, France
1	Prof. Dr. H. Schlichting, Institut für Stromungs, Technische Hochschule, Braunschweig, Germany
1	Dr. Eng. E. Truckenbrodt, Körnerstrasse 12, Braunschweig, Germany
1	Prof. Dr. G. Weinblum, Ingenieur Schule, Berliner Tor 21, Hamburg, Z620, Germany
1	Satish Dhawan, Department of Aeronautical Engineering, Indian Institute of Science, Bangalore 3, India
1	Dr. S. Goldstein, Haifa Institute of Technology, Haifa, Israel
1	Gen. Ing. V. Pugliese, Presidente, Instituto Nazionale per Studi ed Esperienze di Architettura Navale, Via della Vasca Navale 89, Rome, Italy
1	Prof. Busuke Hudimoto, Engineering Research Institute, Kyoto University, Kyoto, Japan
1	Dr. Jun-ichi Okabe, The Research Institute for Applied Mechanics, Kyushu University, Hakozaki-machi, Fykuoka-shi, Japan
1	Prof. J.M. Burgers, Laboratorium Voor Aero- En Hydrodynamica, Nieuwe Laon 76, Delft, The Netherlands
1	Dr. R. Timman, National Luchtvoortlaboratorium, Slaterwag 145, Amsterdam, The Netherlands
1	Office of Scientific Attaché of Netherlands Embassy, 1470 Euclid St., N.W., Washington, D.C.
1	Prof. J.K. Lunde, Skipsmodelltanken, Tyholt Trondheim, Norway
1	Sr. M. Acevedo y Campoamor, Director, Canal de Experienceas Hidrodinamicas El Pardo, Madrid, Spain

Copies

1	Director, Statens Skeppsprovningsanstalt, Göteborg 24, Sweden
1	Director, Aeronautical Research Institute of Sweden, Ranhammersvagen 12, Ulsvunda, Sweden
1	Prof. J. Ackeret, Institut für Aerodynamik Der Eidgenössiche, Technische Hochschule, Zürich, Switzerland
1	Prof. O.J.M. Campos, Jefe de Laboratorio del Instituto Máquinas de la Facultad de Ingenieria, Montevideo, Uruguay
9	British Joint Services Mission, Navy Staff, P.O. Box 165, Benjamin Franklin Station, Washington, D.C.
3	Canadian Joint Staff, Washington, D.C.